FINAL REPORT

Mechanical Chevrons and Fluidics for Advanced Military Aircraft Noise Reduction

SERDP Project WP-1584

MARCH 2011

Dr. K. Kailasanath
Naval Research Laboratory

Dr. Ephraim Gutmark
University of Cincinnati

Dr. Steven Martens
GE Global Research

SERDP
DOD ▪ EPA ▪ DOE

Report Documentation Page

Form Approved
OMB No. 0704-0188

1. REPORT DATE	2. REPORT TYPE	3. DATES COVERED
MAR 2011	**N/A**	**-**

4. TITLE AND SUBTITLE	5a. CONTRACT NUMBER
Mechanical Chevrons and Fluidics for Advanced Military Aircraft Noise Reduction	5b. GRANT NUMBER
	5c. PROGRAM ELEMENT NUMBER
6. AUTHOR(S)	5d. PROJECT NUMBER
	5e. TASK NUMBER
	5f. WORK UNIT NUMBER
7. PERFORMING ORGANIZATION NAME(S) AND ADDRESS(ES) **Naval Research Laboratory**	8. PERFORMING ORGANIZATION REPORT NUMBER
9. SPONSORING/MONITORING AGENCY NAME(S) AND ADDRESS(ES)	10. SPONSOR/MONITOR'S ACRONYM(S)
	11. SPONSOR/MONITOR'S REPORT NUMBER(S)

12. DISTRIBUTION/AVAILABILITY STATEMENT
Approved for public release, distribution unlimited

13. SUPPLEMENTARY NOTES
The original document contains color images.

14. ABSTRACT

There is a growing need to reduce significantly the noise generated by high-performance, supersonic military aircraft. The noise generated during takeoff and landing on aircraft carriers has direct impact on shipboard health and safety issues. Noise complaints are increasing as communities move closer to military bases or when there are changes due to base closures and realignment. Furthermore, U.S. and international noise regulations and policies will have an impact on military operations and training unless we take effective steps to reduce the noise. In response to a statement of need (WPSON-07-04) identified by SERDP, the Naval Research laboratory (NRL) in collaboration with the University of Cincinnati (UC) and GE Aircraft Engines, proposed a three-year research program investigating the use of mechanical chevrons and fluidics for reducing the noise from supersonic military jet aircraft. The technical approach adopted was a combined experimental and computational study. This final technical report provides details of the studies conducted and the results obtained. First, we show that the numerical simulations can accurately predict the details of the flow field and noise generated by supersonic jets from nozzles that are representative of military jet aircraft engine nozzles. Then, we use the numerical simulations and complementary experiments to derive further information on the source of noise from supersonic jets under a variety of operating conditions. With the benefit of this knowledge, we investigate and report on the potential of mechanical chevrons and three fluidics-based techniques to reduce the noise. We find that each of the techniques investigated are capable of providing significant noise reduction but further studies are needed to optimize these techniques and assess a tradeoff between various factors such as cost of implementation, potential impact on performance and benefits derived.

15. SUBJECT TERMS

16. SECURITY CLASSIFICATION OF:			17. LIMITATION OF ABSTRACT	18. NUMBER OF PAGES	19a. NAME OF RESPONSIBLE PERSON
a. REPORT **unclassified**	b. ABSTRACT **unclassified**	c. THIS PAGE **unclassified**	**SAR**	**71**	

Standard Form 298 (Rev. 8-98)
Prescribed by ANSI Std Z39-18

Table of Contents

List of Figures

List of Acronyms and Symbols

A – Speed of Sound

A_e – Exit area

A_t – A* -- Throat area

BBSN – Broadband Shock-Associated Noise

CD – Convergent-Divergent (to describe nozzle shape)

D – D_e – Jet Diameter at nozzle exit

D_j – diameter of a fully expanded jet

dP/dt – time derivative of pressure

GE – General Electric company

L_s – shock cell spacing

LES – Large Eddy Simulation

M_d – Design Mach Number

M_j – Mach number of a fully expanded jet

Mic – microphone

NPR – Nozzle Pressure Ratio, Ratio of pressure upstream of the nozzle to the ambient pressure.

NRL – Naval Research Laboratory

St - Strouhal number

SPL – Sound Pressure Level

OASPL – Over-All Sound Pressure Level

UC – University of Cincinnati

U_j – Axial velocity of fully expanded jet

a_∞ - ambient sound velocity

f – frequency

L_s - shock-cell spacing

p - pressure

p_∞ - ambient pressure

p_{02} - total pressure behind a local normal shock

r - radial coordinate

ρ - density

ρ_∞ - ambient density

u - streamwise velocity

v - vertical velocity

ω - vorticity

x - streamwise coordinate

y - vertical coordinate

ψ - Angle measured from the upstream axial direction

Acknowledgments

The work presented in this report was sponsored by the Strategic Environmental Research and Development Program (SERDP) under Project number WP-1584.

Abstract

There is a growing need to reduce significantly the noise generated by high-performance, supersonic military aircraft. The noise generated during takeoff and landing on aircraft carriers has direct impact on shipboard health and safety issues. Noise complaints are increasing as communities move closer to military bases or when there are changes due to base closures and realignment. Furthermore, U.S. and international noise regulations and policies will have an impact on military operations and training unless we take effective steps to reduce the noise. In response to a statement of need (WPSON-07-04) identified by SERDP, the Naval Research laboratory (NRL) in collaboration with the University of Cincinnati (UC) and GE Aircraft Engines, proposed a three-year research program investigating the use of mechanical chevrons and fluidics for reducing the noise from supersonic military jet aircraft. The technical approach adopted was a combined experimental and computational study. This final technical report provides details of the studies conducted and the results obtained.

First, we show that the numerical simulations can accurately predict the details of the flow field and noise generated by supersonic jets from nozzles that are representative of military jet aircraft engine nozzles. Then, we use the numerical simulations and complementary experiments to derive further information on the source of noise from supersonic jets under a variety of operating conditions. With the benefit of this knowledge, we investigate and report on the potential of mechanical chevrons and three fluidics-based techniques to reduce the noise. We find that each of the techniques investigated are capable of providing significant noise reduction but further studies are needed to optimize these techniques and assess a tradeoff between various factors such as cost of implementation, potential impact on performance and benefits derived.

Objective

The need to develop effective approaches to reduce significantly the noise generated by high performance, supersonic military aircraft engines was identified by SERDP. In response, we developed a combined experimental and numerical approach to better characterize the source of the noise and investigate several promising techniques to reduce the noise. The specific objectives of this research were two fold. First, to develop physical understanding of the mechanisms of noise production and identify noise sources when a military aircraft engine is operating at ideal (perfectly expanded) and non-ideal conditions (over and under-expanded nozzle exhaust). Second, to develop three fluidically-based noise reduction techniques that can: a) enhance effectiveness of mechanical chevrons, or b) induce virtual modification of the nozzle area ratio to ensure continuous adaptation to design conditions, or c) use fluidic jets in a regular nozzle to virtually mimic mechanical elements such as chevrons.

Background

There is a growing need to reduce significantly the noise generated by high performance, supersonic military aircraft. Community noise complaints are increasing as communities move closer to military bases and military aircraft begin to use conventional airports. The noise

generated by military aircraft also has direct impact on ground and shipboard health and safety issues including pilot and ground crew comfort, in addition to the military requirement of low detectability. Furthermore, U.S. and international noise regulations and policies will have an impact on the operations and training unless effective steps are taken to reduce the noise.

There is a significant amount of literature dealing with noise reduction in civilian, subsonic aircraft. Some of the techniques found effective for subsonic aircraft could be applied for noise reduction in supersonic jets. Many of these techniques use flow modifiers such as mechanical chevrons to enhance the mixing of the core jet with the fan flow or the combined flow with the surroundings and reduce the radiated noise. A distinct difference between civilian aircraft engines and advanced military aircraft engines is that military engines tend to have low bypass ratios (ratio of flow through outer regions of the jet engine to that through the core of the engine) and high velocities, and thus their noise tends to be dominated by jet exhaust noise, especially shock-associated noise. During certain flight conditions, such as during takeoff or landing, the exhaust from these engines tends to be non-ideally expanded (overexpanded when the exhaust pressure is below ambient and underexpanded when the pressure is above ambient). Non-ideally expanded exhaust flows contain shock cells in the jet exhaust, causing high-amplitude screech tones and broadband shock-associated noise, components that increase the overall noise level. Therefore, this research was focused on understanding these non-ideally expanded exhaust flow conditions and characterizing the noise sources, so that noise reduction techniques may be successfully pursued. The approach adopted was a combined experimental and computational study.

Numerical simulations can, in principle, play a significant role in the test and evaluation of various noise reduction concepts. However, for the results of these simulations to be credible, they need to be first compared and evaluated against relevant experimental data. This should include geometries and flow conditions that are representative of realistic engine configurations and operating conditions. This is a very challenging task. Our first task in this project was to show that our numerical simulations could accurately capture the flow field and near-field noise from representative jet engine nozzles and indeed this was a go/no-go decision point in the overall project plan.

Although there are still fundamental questions about the source and mechanisms of noise in supersonic jets, significant progress has been made over the past few decades [for example, Refs. 1-25]. From the previous studies, it is known that the noise generated by an imperfectly expanded supersonic jet flow consists of discrete and high amplitude screech tones, broadband shock-associated components and mixing noise. The first two types of noise are related to the shock waves that are present in the high-speed jet flow. While the mixing noise dominates in the downstream direction, the shock-associated noise elevates the overall noise level in the upstream direction. The screech tones are thought to arise due to a feedback loop involving the large-scale flow structures, their interactions with the shock-cell structure and flow disturbances at or near the nozzle lip. Therefore, for the problem at hand, the simulations will need to accurately capture shock waves, unsteady large-scale flow structures and their interactions. The focus of this project is on accurately characterizing the flow field and near-field noise generated. When needed, the far-field noise information can be obtained from the near-field data using traditional approaches presented in the literature [26, 27].

Technical Approach (Materials and Methods)

This was a joint research effort with experiments being conducted at the University of Cincinnati (UC), numerical simulations at the Naval Research Laboratory (NRL) and overall guidance and design help from the General Electric Global Research Center (GE). Our technical approach was to design and fabricate representative nozzles, conduct experiments and acquire data, compare this information and validate numerical simulations, and then use both experiments and simulations to understand the sources of the noise and investigate three fluidics-based approaches to reduce the noise. All these tasks have been successfully completed and the results are described in the next section.

The scale-model laboratory experiments were conducted in the Aeroacoustic Test Facility (ATF) at UC. This is essentially a 24' by 25' anechoic room that has been found to be anechoic down to 400 Hz. Eight or Ten B&K ¼" free-field microphones are placed on a circular arc at a distance of 51D (diameters) from the nozzle exit. These microphones are arrayed at angles from 35° to 150° measured from the upstream direction. The microphones are sampled at 200 kHz and corrected for the presence of protective grid caps. This grid cap correction becomes large above 80 kHz, but the range from 400Hz to 80 kHz is adequate to observe the physically significant spectral characteristics. Figure 1 shows the experimental set up in the UC test facility.

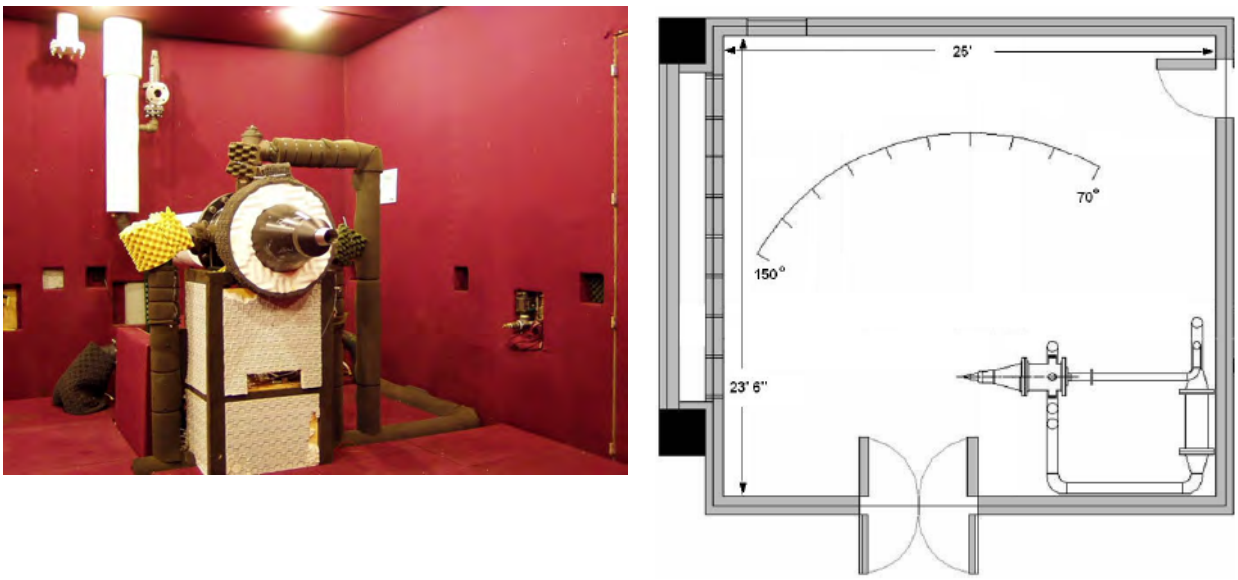

Figure 1. Experimental set up in the anechoic chamber at UC for the far-field measurements. One of the nozzles for the experiments is shown installed in the figure on the left.

In addition, near-field measurements are also being taken in the same facility (please see Figure 2 for details]. For these, measurements, eight B&K ¼" free-field microphones were mounted on rake at 6.25" intervals. The rake is then mounted on a traverse and moved by 1.042" steps along its length and at 1" intervals along a radius from the jet axis. This results in a grid of 11 x 66 measurement locations on an approximate 1" square grid. Two such grids are established. One grid, the upstream grid has its near edge 1" from the shear layer location for the under-expanded jet, with the upstream-most microphone in the exit plane of the nozzle. This grid is canted at a divergence angle of 10° to follow the approximate divergence angle of the jet. This location was checked to assure that the microphones did not protrude into the jet itself. A second grid, the downstream grid, has its upstream-most microphone in the same location as the downstream most microphone in the first grid. The second grid extends the measurement region farther downstream.

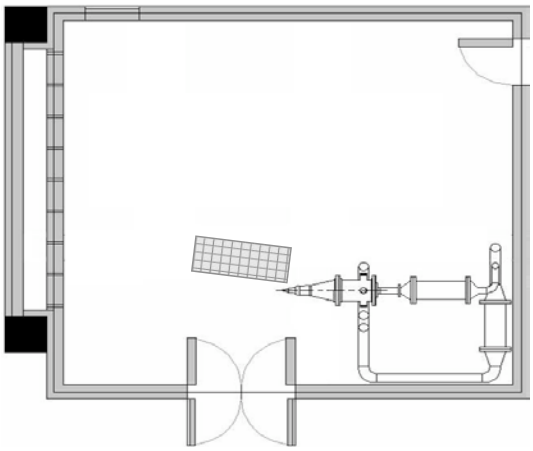

Figure 2. Plan view of the facility showing the near-field measurement locations.

In addition to these acoustic measurements, centerline pressure, PIV measurements and shadowgraph visualizations of the flow field have also been conducted to characterize the sources of the noise and to provide data to compare with results of numerical simulations.

The numerical simulations at NRL are being conducted using an unstructured grid based, finite element flow code, FEFLO, developed and tested for a variety of flow problems. The use of unstructured grids or meshes consisting of tetrahedral elements in three-dimensions, allows us to represent complex geometrical details. The flow solver used is a high order, monotonicity-preserving scheme, FEM-FCT [28] that has been shown to capture shocks and other discontinuities that may arise in compressible flows [29]. During the first year of this project, the code was modified and adapted to simulate the non-ideal (under and over-expanded jet) behavior of supersonic jets issuing from a variety of nozzle configurations. Information on the geometry of the nozzle configurations was obtained from UC and different meshes were generated to represent the geometry and flow field. Unsteady, three-dimensional simulations were carried out. These simulations are in the category of implicit large-eddy simulations called Monotonically Integrated Large Eddy Simulations or MILES [30]. Before comparison with experimental data, the effect on the solutions of various parameters such as mesh size and distribution, boundary conditions, implicit numerical diffusion and other numerical parameters were studied.

Computational diagnostics that are similar and complementary to diagnostics used in the experimental set up were also developed and tested with existing experimental data. In the simulations, data is gathered from within the flow field since the simulated probes are inherently non-intrusive. Data gathering locations (as represented by the grid) from a representative under-expanded CD nozzle flow simulation is shown in Fig. 3. Information on the flow field (e.g., density, vorticity, velocity) including the local unsteady pressure fluctuations has been gathered at the various numerical probe locations (all the grid intersection locations, shown below in Fig. 3). In the background of Figure 3, the flow field in terms of the calculated density is also shown for reference.

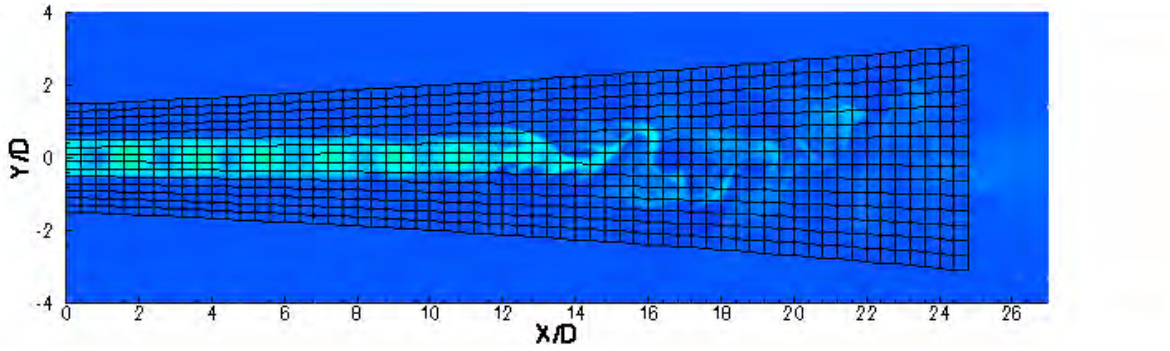

Figure 3. Distribution of numerical probes in a CD nozzle flow field simulation.

Detailed simulations have been carried out of the flow field and noise generated by one of the CD nozzles under different operating conditions. The results from the simulations have been compared with experimental data acquired at UC. After successful validation of the numerical approach, both the simulations and experiments were used in a complementary manner to characterize the sources and mechanisms involved in the generation of noise from supersonic jets issuing from nozzles representative of high-performance military aircraft. Then the effectiveness of mechanical chevrons and fluidics for noise reduction under a variety of conditions were investigated using experiments and numerical simulations.

Results and Accomplishments

The overall results and accomplishments from this project can be presented in various ways. For consistency with other project documentation, it is broadly divided into the same categories as the four major technical tasks within this project. To summarize, the four major tasks were: 1) Verification and Validation studies to establish the accuracy of the Computational Approach; 2) Conducting experiments and simulations for identifying and characterizing the noise sources and mechanisms; 3) Development of noise reduction technologies, especially those based on fluidics and 4) Synthesizing results and developing recommendations.

Task 1: Baseline Verification and Validation Studies

A critical part of the overall project was establishing that the computed flow field is an accurate representation of the actual supersonic jet flow from typical military aircraft engine nozzles. This task was divided into five sub-tasks: a) design and fabrication of the baseline nozzle configurations representative of military jet engine nozzles, b) adapting the computer code for noise simulations and representing the nozzle configurations, c) development of computational diagnostics, and d) setting up and acquiring experimental data and e) comparing the results from the numerical simulations to those acquired in the experiments.

The first key step was to design and fabricate representative supersonic converging and converging-diverging (CD) nozzles at UC with design guidance from GE. Four nozzles were developed for this project. One is a pure convergent nozzle, and the other three are convergent-divergent nozzles typical of tactical military jet variable geometry nozzles. Such geometries are not the contoured "method of characteristics theory-based" nozzles often seen in the literature. They are nozzles with a conic contraction section, a sharp throat and a conic expansion. Such geometry is required represent the variable geometry mechanism used on tactical military jets currently in the field. The four nozzles have design Mach numbers (M_D) of 1.0, 1.3, 1.5 and 1.65. The design Mach number represents the physical area ratio of each nozzle. Experiments were conducted and data acquired at UC with all these nozzles for a variety of operating conditions.

Unsteady, three-dimensional simulations were carried out at NRL for the nozzle geometries provided by UC and GE. Before comparison with experimental data, "verification" simulations were carried out to understand the impact of various numerical parameters on key quantities that are characteristic of the flow field. The verification studies included tests of the effects of the grid resolution, mesh distribution, numerical parameters (e.g., flux limiters), domain size and various boundary conditions on the computed solution. These studies showed that the solutions were computed accurately. The grid-resolution studies are discussed below as a representative example of the verification studies.

Three grid resolutions were used to evaluate the dependence of the key features of the flow on the numerical grid distribution. Besides the grid resolution of 0.0345D (where D is the jet exit diameter), two coarser meshes that have cell sizes of 0.044D (25% coarser) and 0.061D (75% coarser) were also tested. Since the lip thickness is very small, cell sizes of the three meshes are reduced gradually near the nozzle exit to have one element around the nozzle lip, and the grid resolution is similar for these three meshes within the range of 1.8D downstream of the nozzle exit. No further attempts were made to further reduce the mesh size around the nozzle lip because it would reduce the time-step size, which in turn would require a much longer computation time. Therefore, this grid resolution study only focused on the region away from the nozzle exit. Figure 4 shows distributions of the centerline static pressure (normalized using the background pressure) using the three meshes for a typical over-expanded case (NPR = 3.5) and one representative under-expanded case (NPR = 4.0). For reference, the nozzle design NPR is 3.7. The agreement over the first two shock cells is very good for all meshes. However, roughly from the location of 4 jet diameters (4D), the results from the 75% coarser mesh start to deviate from the predictions of the two finer meshes. On the other hand, the difference between the two

finer meshes is small. Comparisons of the noise spectra predicted by the three grid resolutions at the location of 2.2D downstream of the nozzle exit and 1D above the jet centerline show good agreement. The comparison of the centerline pressure results and the spectra data indicate that simulations using the two finer meshes have approximately achieved grid independence, at least at the level of mean flow quantities and acoustic spectra. To be on the conservative side and in order to capture more small-scale turbulence structures, the finest mesh of the three was used for all the results discussed below and in the rest of the project.

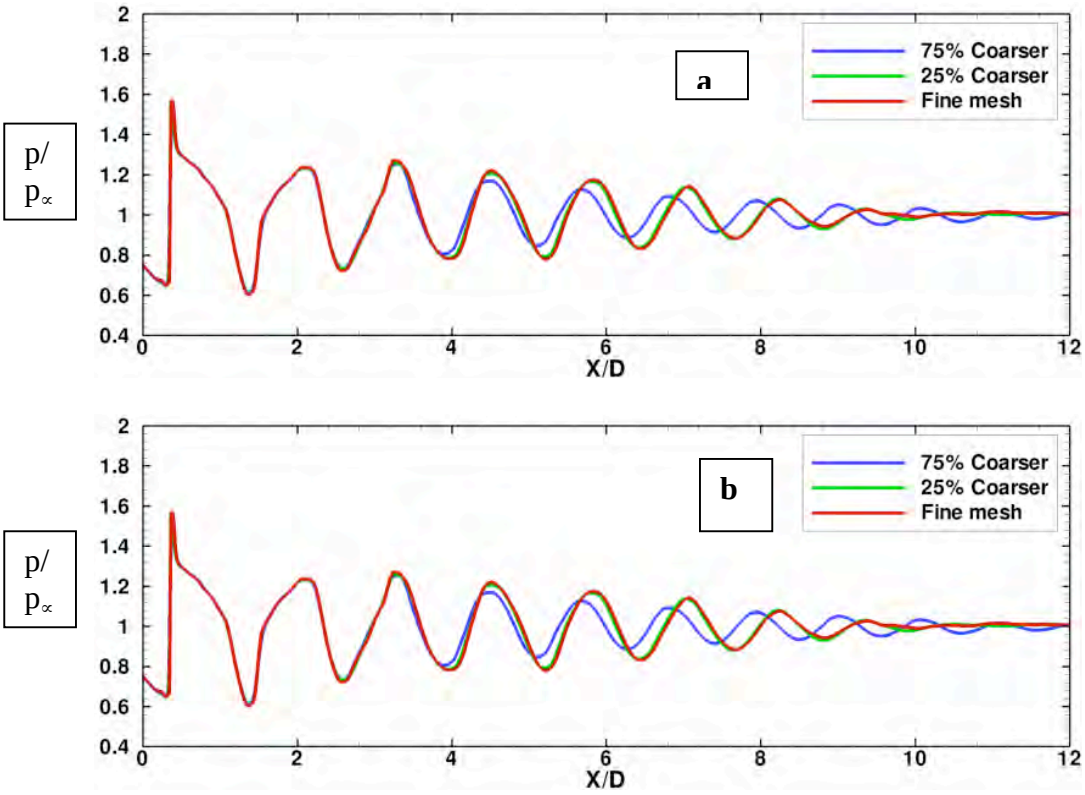

Figure 4. Spatial distributions of the normalized centerline static pressure predicted using three grid resolutions for the cases with: (a) NPR = 3.5. (b). NPR = 4.0.

The output of the numerical simulations is a detailed distribution of all the flow variables (e.g., pressure, density, different components of the unsteady velocity) at each of the grid points at each computational time step. This is an enormous amount of data to store and digest since a typical simulation of the nozzle flow field involves about 10-15 million grid points. Therefore, computational diagnostic tools were developed to capture key features of the flow field. In some cases they are to obtain data similar to those obtained in experiments and for use in direct comparisons. In other cases, they are complementary to the data obtained in experiments and enable a more complete characterization of the flowfield. For example, it is not feasible to insert the pressure probes discussed above directly into the supersonic flowfield without modifying the flow while it is not currently possible to capture the pressure in the far field directly in the simulations. The map of the near field and far field noise measurements along with the

information from the unsteady pressure fluctuations in the flow field from the simulations can be used to better characterize the noise sources in the flow field. Various computational flow diagnostics were developed at NRL and a variety of them will be utilized in discussing the project accomplishments in this report.

After the verification studies which concluded that the computed solutions were sufficiently independent of the grids, domain size, boundary conditions and other numerical parameters, the focus was shifted to validation studies. The purpose of the validation studies is to ascertain if the computed results are a good representation of the actual physical problem of interest. Hence, the results were compared with carefully conducted representative experiments. A summary of the experimental tests conducted is provided below in Figure 5.

Pressure Ratio	Fully Expanded M_J	M_D 1.0 AR 1.000	M_D 1.3 AR 1.067	M_D 1.5 AR 1.181	M_D 1.65 AR 1.295
1.50	0.78	subsonic	subsonic	subsonic	subsonic
1.89	1.00	perfect			
2.00	1.05	under	inside	inside	inside
2.50	1.22	under	over	over	inside
2.79	1.30		perfect		
3.00	1.36	under	under	over	over
3.50	1.47	under	under	over	over
3.70	1.50	under	under	perfect	over
4.00	1.56	under	under	under	over
4.50	1.64	under	under	under	over (*)
4.61	1.65				perfect (*)
5.00	1.71	under	under	under	under (*)

* indicates that channel 8 at 150° was slightly clipped

Figure 5. Parameters for the Experimental test matrix.

The computed solutions for both under-expanded and over-expanded jets were then compared with experimental data and shown to be in good to excellent agreement. Representative comparisons of the centerline pressure distributions are shown in Figure 6 for the over-expanded jet with the nozzle pressure ratio (NPR) of 3.5 and for an under-expanded jet with NPR of 4.0 in Figure 7. Considering the difficulties in making accurate measurements in these high-speed flows (especially correcting for the shocks introduced by the), the comparisons must be considered to be good. Other quantities compared included shock-cell size, size of the potential core, extent of jet mixing, Mach number distribution, shadowgraphs, noise spectra including key frequencies and characteristic differences in the flow field between under- and over-expansion. A comparison of the shock-cell spacing predicted by the large-eddy simulations (LES), measured by experiments and predicted by Prandtl's vortex sheet model is shown in Fig. 8.

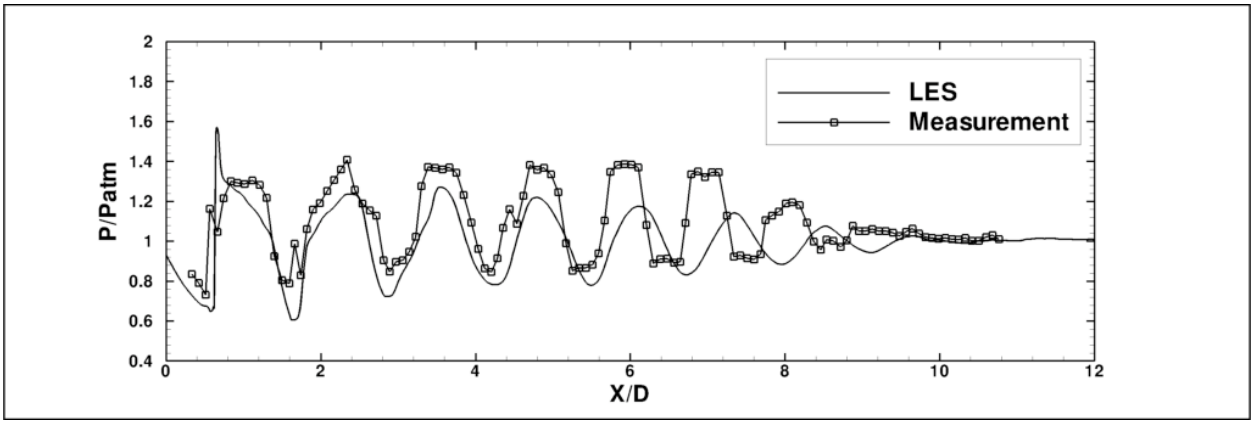

Figure 6. Comparison of the centerline pressure distributions predicted by the simulations at NRL to those from the experiments at UC for the over-expanded jet with NPR = 3.5.

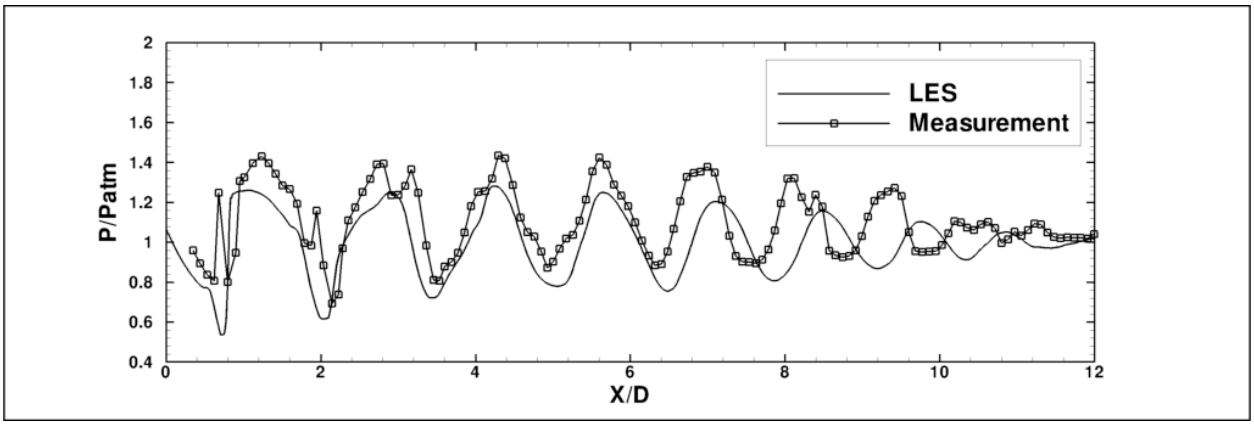

Figure 7. Comparison of the centerline pressure distributions predicted by the simulations at NRL to those from the experiments at UC for the under-expanded jet with NPR = 4.0.

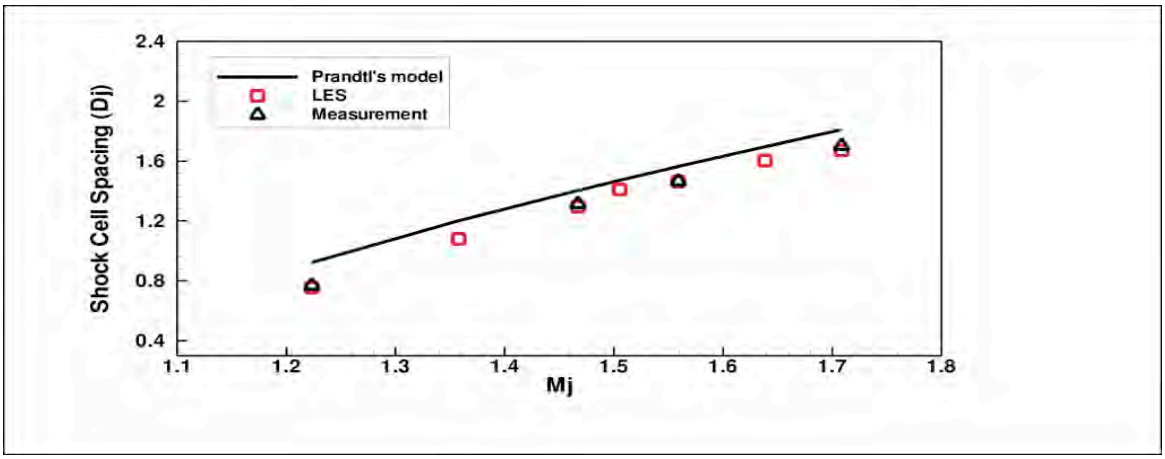

Figure 8. Comparison of the predicted variation (red squares) in the shock-cell spacing with increasing jet Mach number (directly related to increase in NPR) with a theoretical model (black line) and experimental data from UC (black triangles).

The comparison between results from the simulations and the experimental measurements is excellent. Although the vortex sheet model slightly over predicts the shock-cell spacing, the trend is in good agreement. It is clear that the shock-cell spacing increase as the total pressure ratio increases and hence the jet Mach number increases. Comparison of the predicted velocity profiles at various axial locations with those measured in the experiments is shown in Fig. 9. Again, the agreement is very good.

In addition to details of the flow field, various measures of the noise have also been compared. For example the noise intensity [as represented by the sound-pressure level (SPL)] at the screech tone frequency is compared in Figure 10. The agreement between the prediction of LES and laboratory is very good.

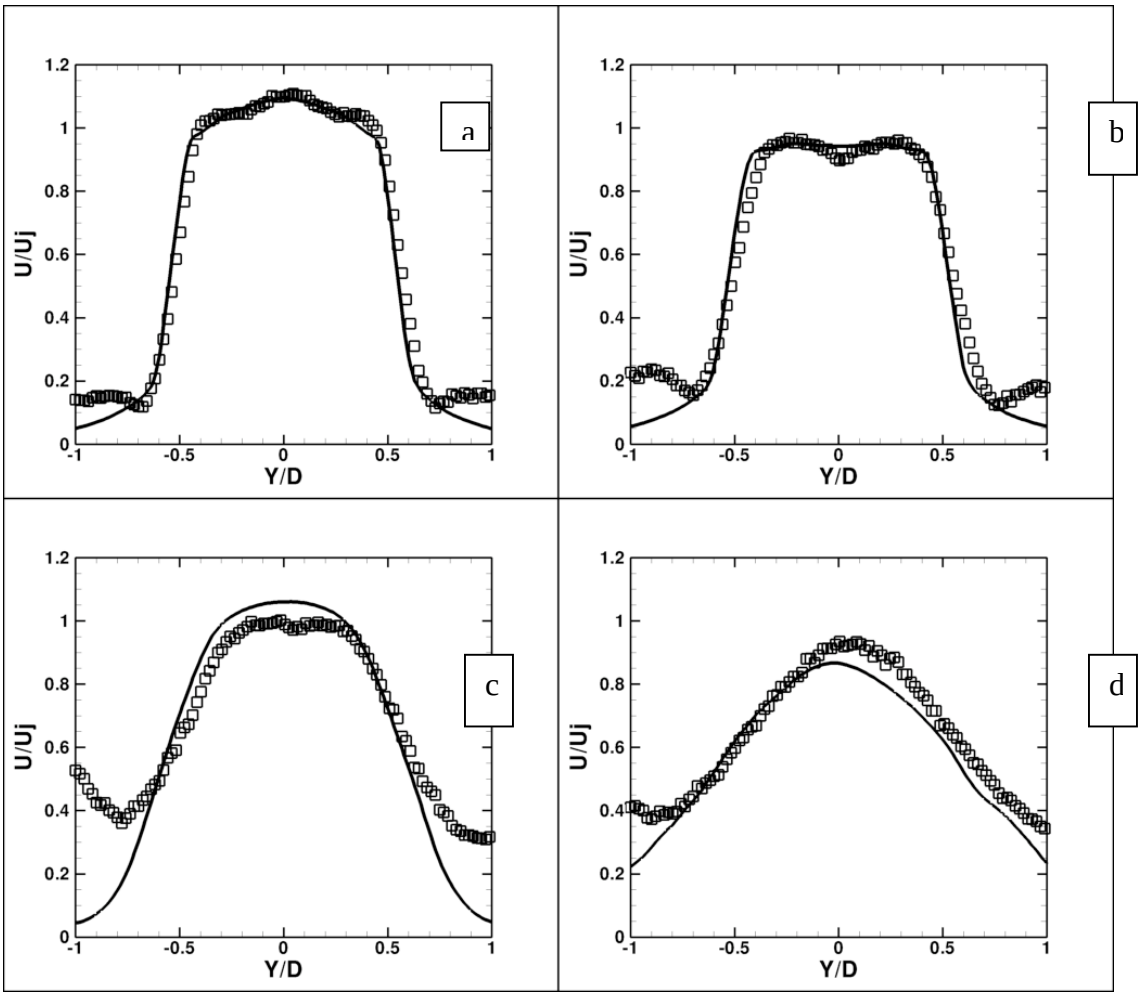

Figure 9. Comparisons of streamwise velocity profiles at four axial locations for the case with NPR=4.0. Lines: LES, symbols: measurement. a). *x = 2.15D*), b). *x = 2.8D*, c). *x = 7.7D*, d). *x =12D.*

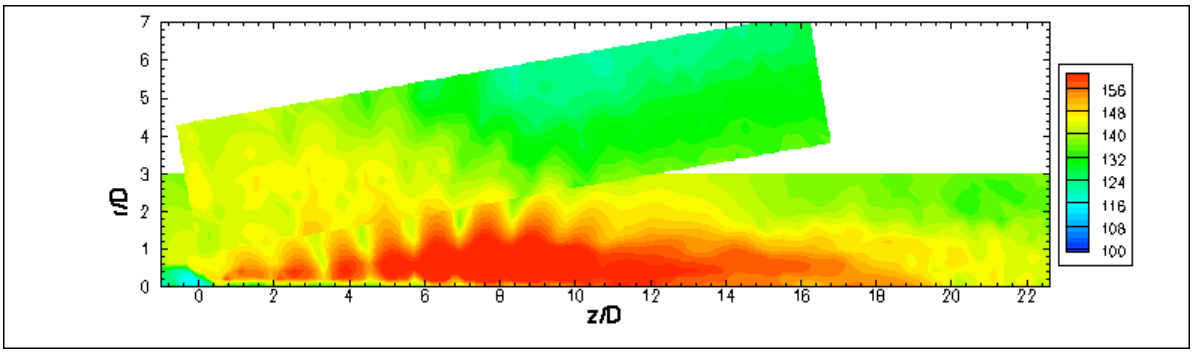

Figure 10. Comparison of the intensity (sound pressure level-SPL) of screech tones for an under-expanded jet, NPR = 4.0. Experimental measurements in the upper angled block and LES in the lower block.

Based on such comparisons, the ability of the simulations to characterize under- and over-expanded jets was demonstrated convincingly. This was the go/no-go decision point and the project was approved for continuation after the interim progress review in February 2008. Various details of these studies have been presented at technical meetings of scientific and professional societies and also archived in a journal publication. One landmark paper [24] received a 2009 Alan Berman Research Publication Award from the Navy. Detailed citations for all publications are provided in the Appendices.

Task 2: Characterize Noise Sources and Mechanisms

After the validation tests were completed successfully, both the experiments and simulations were used to develop better physical understanding of the mechanisms of noise production and identify noise sources when a military aircraft engine is operating at ideal and non-ideal pressure expansion conditions (over- and under-expanded nozzle exhaust). This was the second major task identified in the project plan.

Analysis of the sound production and radiation at several characteristic frequencies were carried out. As seen in Figure 10, an overlay of the narrow-band spectra (SPL) at a characteristic (screech) noise source frequency shows a smooth transition from the computed solutions to the experimental data, indicating that both computations and experiments are capturing the same noise source. The smooth transition in the overlay is a significant accomplishment because experimentally it is not possible to interrogate the noise source non-intrusively and we must rely on the computations for this information. The perceived noise at a distance is a parameter that can be best measured experimentally and is prohibitively expensive to compute directly. The current work has highlighted the complementary role of the experiments and simulations.

The nozzle used for most of the experiments and simulations has an area ratio of 1.181 corresponding to a design Mach number, M_d, of 1.5. The design condition for this nozzle is thus a Nozzle Pressure Ratio (NPR) of 3.671, which will achieve perfect expansion. Experiments and Simulations have been completed for the design condition (NPR = 3.67) as well as three NPR (2.5, 3.0, and 3.5) lower than the design point and as well as three pressure ratios (4.0, 4.5 and 5.0) higher than the design point. These results conclusively establish that the flow is not shock-

free even at the design point due to the waves generated from the sharp transition from the converging section to the divergent one at the throat of the nozzle. Discrete, high magnitude screech tones are present for all cases, except in the simulations of the case with NPR of 2.5. A distinct feature of this case is a near normal shock just outside the nozzle. The magnitude of the screech tone is lowest for the design condition (NPR of 3.7). The variation of the computed screech frequency with NPR (and hence, jet Mach number) is in general agreement with theoretical predictions (based on Tam et al. [31]) and in even better agreement with experimental data as shown in Figure 11.

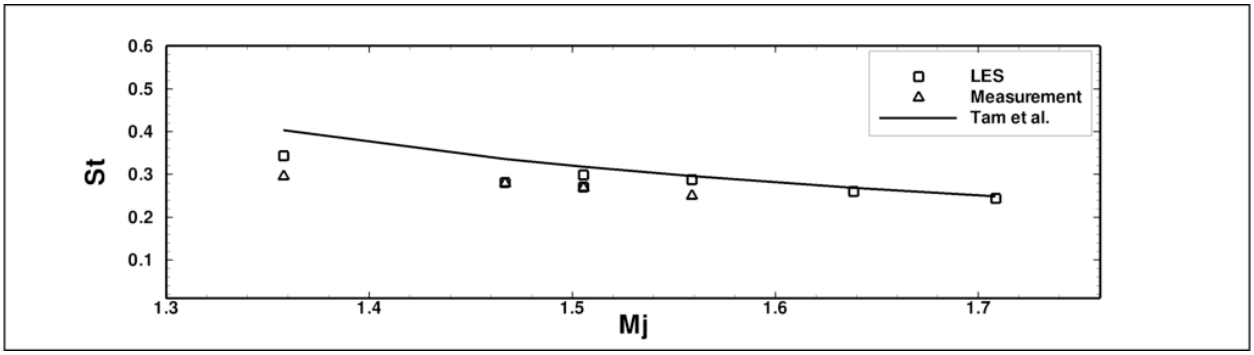

Figure 11. Strouhal number $St = \frac{f D_j}{U_j}$ of the screech frequency versus fully expanded jet Mach number as predicted by the Large-Eddy Simulations (squares), experimental measurements (triangles) and a standard theory (line).

Looking at spatial distributions of the instantaneous pressure (Fig. 12) and its time derivatives (Fig. 13) have been very helpful, especially when viewed as an animation (movie). Representative still-frames from the movies are shown in Figs. 12 and 13. Apart from the features of the flow that have already been discussed, such as the shock cells, fluctuations of shock cells and banded structures of the screech tones are observed. Another interesting feature is the presence of small pressure pockets from the nozzle lip to several diameters downstream. Those pressure pockets are signatures of the large-scale coherent turbulent motions. The movie files of the instantaneous static pressure show that small pressure pockets are disturbances generated at the nozzle lip that propagate downstream. They interact with shock cells and grow rapidly through this interaction. Sometimes they merge as they propagate. The time derivatives of the static pressure show these details better than the pressure itself, since time derivatives measure pressure fluctuations and amplify the high frequency information. It can be seen from distributions of the time derivatives that those large-scale coherent motions start from the jet lip-line and gradually grow into the jet core and finally occupy the jet completely. This occurs roughly at 4D (the beginning of the third compression cell) for NPR = 4.0 and between 3D and 4D (after the fifth compression cell) for NPR = 2.5. From these locations, till the end of the potential core, which is 12D for NPR = 4.0 and 9D for NPR = 2.5, the interaction between the shock cells and the coherent motions becomes very strong and large perturbations of the shock cells are seen. The interaction between the coherent motions and the shock cells generate a screech tone in all cases except for NPR=2.5, where this interaction is not sufficient to generate the screech tone. Another prominent feature is that the near field is populated with waves with short wavelengths and high frequencies. They can be seen near the nozzle lip region, in the

propagation paths of coherent motions, in the region where the coherent motions interact strongly the shock cells, and finally in the mixing region.

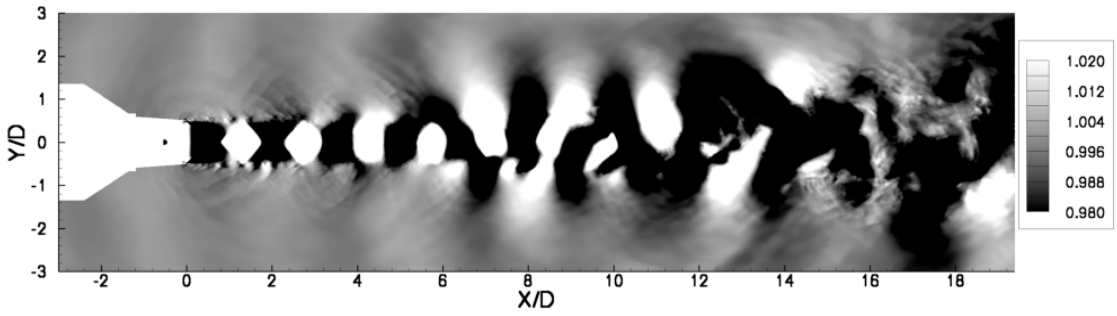

Figure 12. Instantaneous distribution of the normalized static pressure (P/P_{∞} .) in the *x-y* plane for NPR = 4.0.

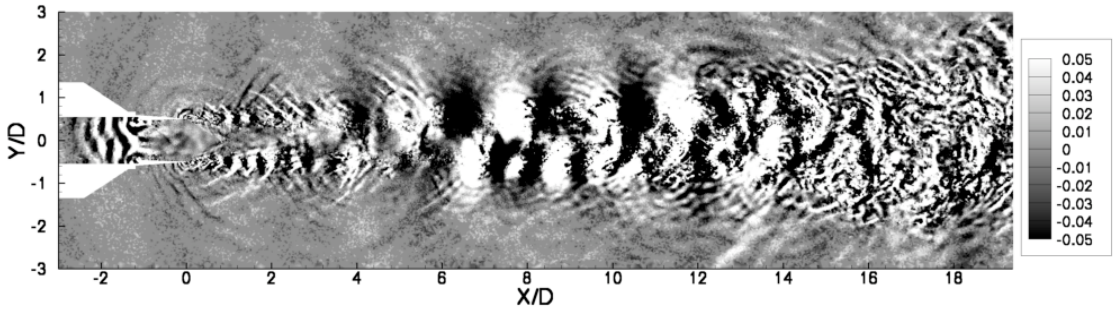

Figure 13. Instantaneous distribution of the time derivative of the static pressure in the *x-y* plane for NPR = 4.0.

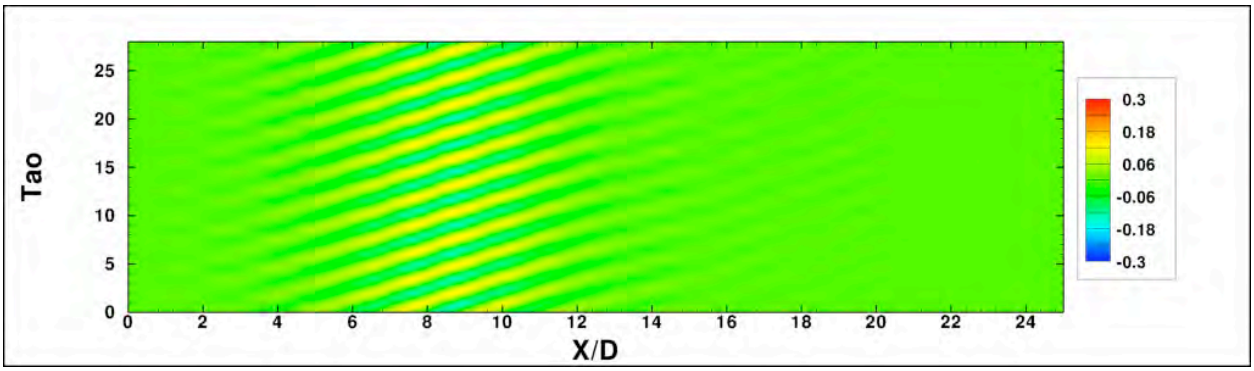

Figure 14. Space-time cross-correlation between the pressure fluctuations at a location outside the jet (2D) with local velocity fluctuations within the jet. The non-dimensional time (Tao) on the y-axis is given by a product of the actual time and the ambient sound-speed divided by the jet exit diameter, D.

Another interesting diagnostic developed was the cross-correlations of the pressure fluctuations outside the jet with the axial velocity fluctuations within the jet. A typical example is shown in Figure 14. Such studies reveal that the screech tone is strongly related to the flow

events occurring between the third shock cell and the end of the potential core (axially 5 to 12 D in Figure 14). The shock-cell spacing itself increases as NPR (and hence jet Mach number) increases. This is consistent with the reduction in screech frequency noted with increasing NPR. The pressure-pressure correlations show that pressure above the nozzle exit is correlated with waves propagating both upstream and downstream. The waves propagating upstream have a speed slightly larger or very near the speed of sound. However, the waves propagating downstream have a speed smaller than the sound speed, but the speed increases as the radial distance increases and reaches the sound speed at a larger radial distance. The time histories of pressure at the jet lip-line and at a higher radial distance reveal cancellation and reinforcement between waves propagating upstream and downstream. This interaction produces waves with shorter wavelengths in the streamwise direction, and the locations of these waves move downstream as the radial distance increases. Further Analysis of the sound pressure level distributions reveals that low frequency noise dominates the mixing region downstream of the potential core.

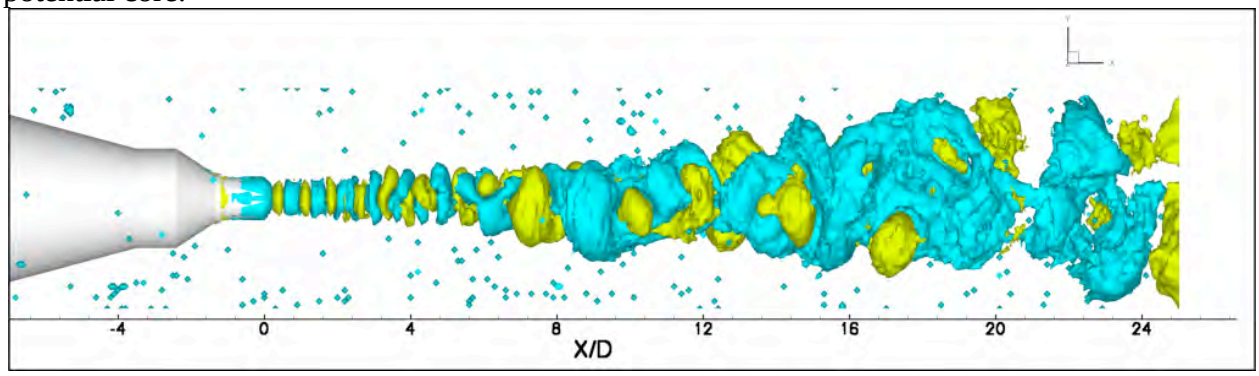

Figure 15. Iso-surface of the static pressure for the case with NPR = 2.5 in the downstream direction of the nozzle exit.

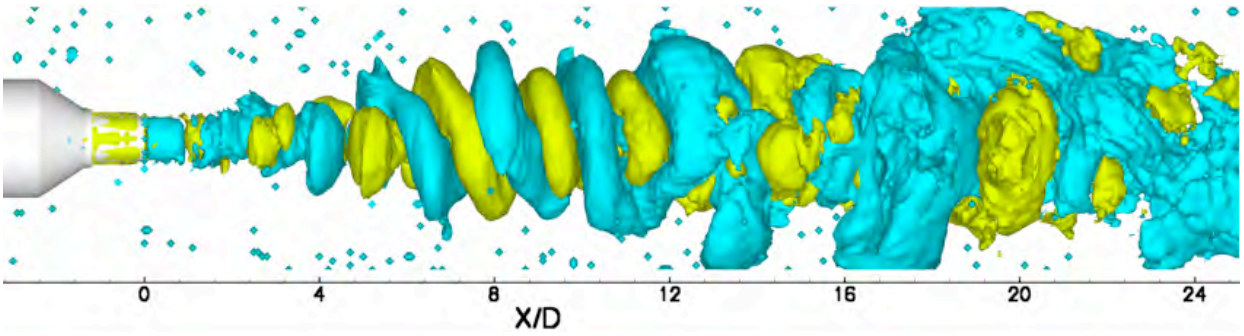

Figure 16. Iso-surface of the static pressure for the case with NPR=4.0 in the downstream direction of the nozzle exit.

The shape of the various observed modes is revealed by looking closely at the iso-surfaces of the static pressure at various levels. For example, Fig. 15, presents iso-surfaces of the static pressure for NPR=2.5 and Fig. 16, the corresponding information for the case with NPR=4.0. It can be seen that the iso-surface at the pressure level (1% of the ambient pressure) is in helical shape for NPR=4.0, but is toroidal in shape for the case with NPR=2.5, where a screech tone is not observed in the simulations. Further analysis of the pressure distributions at various axial

locations at different times clearly shows that the pressure fluctuations rotate in a clock-wise pattern.

From all these studies, we can draw some general observations. Overall, noise generation can be divided into three major regions according to the dominant mechanism of noise generation. The first is the area near the nozzle lip and several diameters downstream. The shock cells are quite stationary in this region, and the main noise contributors are the nozzle lip and the propagation of the large-scale coherent motions. They mainly contribute to high frequency noise. The second region is the place where the interaction between the coherent structures and the shock cells is strong and large pressure fluctuations are seen. In addition, high-frequency noise is also generated by the large pressure fluctuations. The first two regions are responsible for the broadband noise generation in shock-containing jets. The third region is the mixing region, where the mixing mechanism is the major noise generator and it contributes mostly to the low-frequency noise.

Task 3: Investigation of Noise reduction techniques

The third task in the project plan was to investigate specific noise reduction strategies involving mechanical chevrons and fluidics. First, we have conducted experiments and simulations to assess the impact of mechanical chevrons on the flow field and near-field noise. Although the emphasis of our noise reduction strategy is based on fluidics, we needed to do these basic studies on chevrons to provide a baseline to evaluate the impact of fluidics-based techniques operating on chevrons or replacing chevrons. For these purposes, further experiments and simulations have been conducted on jets from a nozzle modified with chevrons (as shown in Fig. 17 for one particular configuration that includes fluidics installation) operating under nominally ideal or perfect-expansion conditions as well as more realistic, non-ideal expansion conditions (more representative of takeoff and landing conditions).

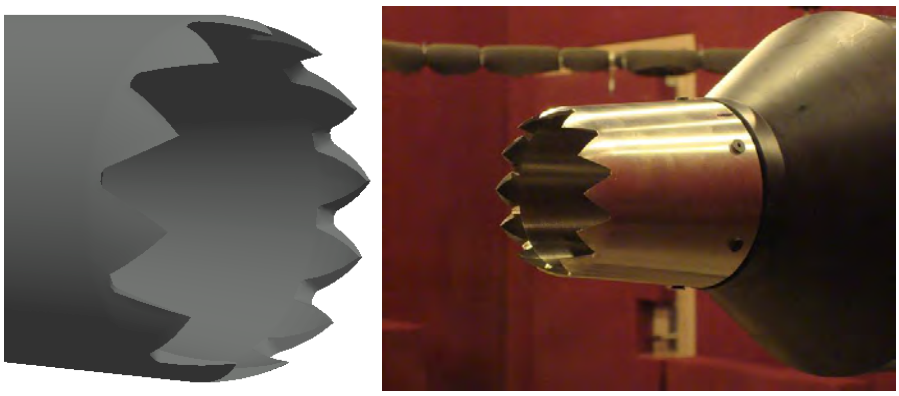

Figure 17. Geometry of the chevron nozzle

Impact of Mechanical Chevrons

Simulations have been carried out by NRL with the chevron nozzle geometry information provided by UC and GE. Figure 18a shows the comparisons of the static pressure and the streamwise velocity between the chevron nozzle and the baseline nozzle.

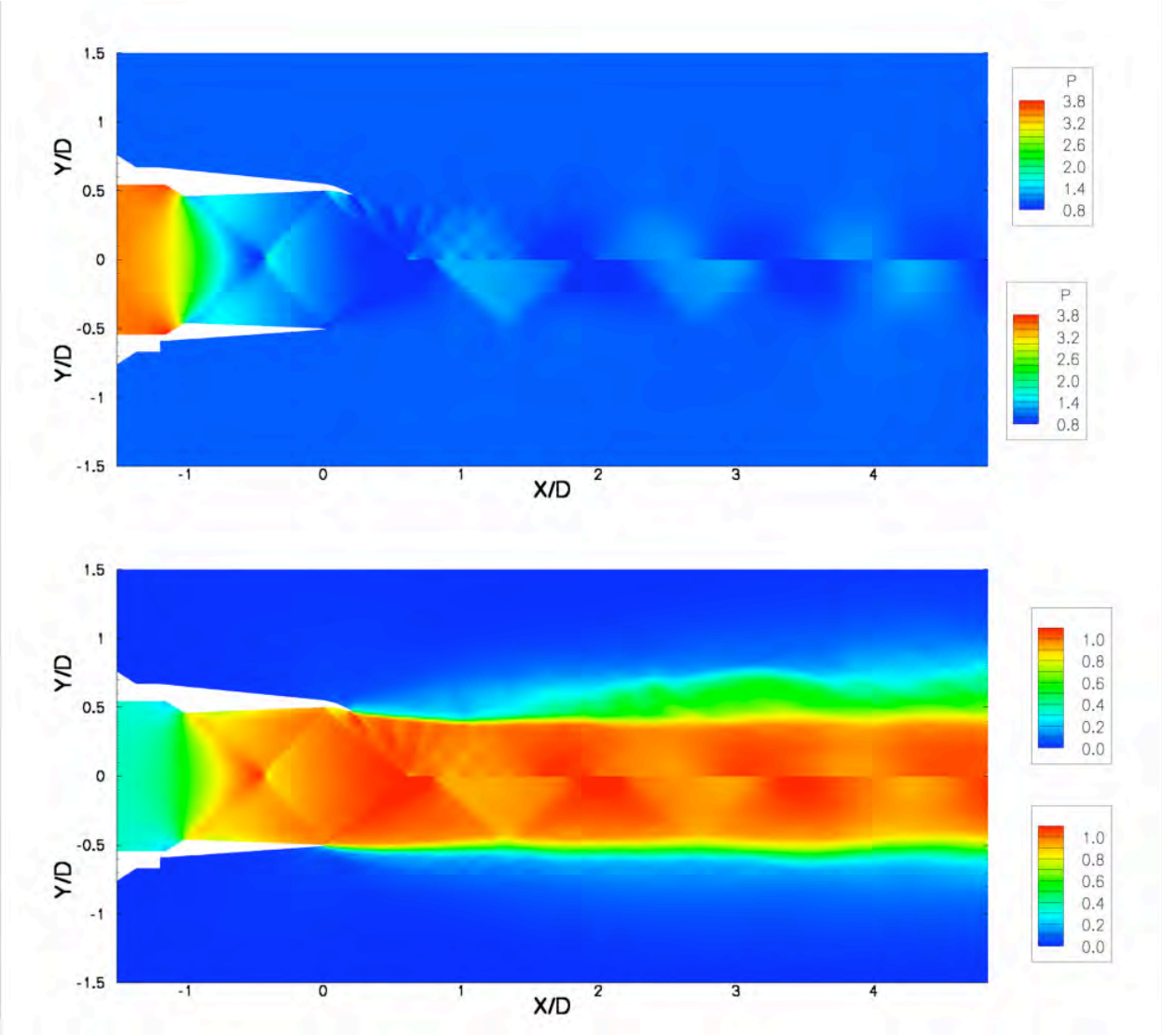

Figure 18a. Impact of chevrons on the static pressure distribution (top) and normalized streamwise velocity distribution (bottom). In each figure, the upper half is from the simulation with chevrons and the lower half is from the baseline case simulations.

It can be seen from the figure that chevrons cause the shock cells to move closer to the nozzle and reduce the spacing between them. In addition, they induce more spread of the jet flow and decrease the strength of the shock cells.

These phenomena have been also observed in the experimental measurements. Figure 18b shows PIV measurements with and without chevrons in the region near the nozzle. The chevron images start further downstream than the baseline so that laser reflections from the chevrons would not impact the results. Similar to the simulations, the figure shows that the shock cells shifted upstream by the presence of chevrons. It also shows the substantial increase in the thickness of the mixing layer and that the chock structures are the same in both the plane through the chevron tips and chevron valleys. This implies that despite the crenellation of the shear layer the shocks remain conical, even after reflecting from the shear layer.

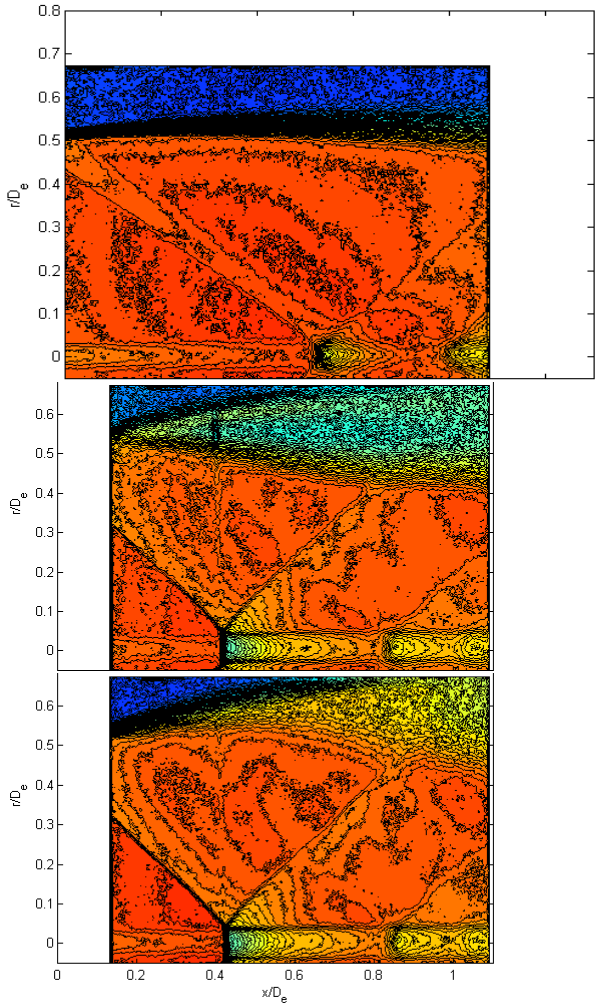

Figure 18b. PIV measurements of axial velocity with and without chevrons. The baseline nozzle (top frame) a plane through the chevron tips (middle frame) and a plane through the valley between the chevrons (bottom frame).

Next, we look at additional local flow field modifications introduced by the mechanical chevrons. Figure 19 shows the static pressure distribution and Figure 20, the velocity vector field in the *yz*-plane at x = 0.1D, which is located at the half way point between the chevron base and tip. Counter-rotating streamwise vortices are seen around the chevron lobes, creating local high-pressure and low-pressure regions circumferentially near the edge of the jet potential core. The streamwise vortices carry high-speed jet fluid out of the potential core and produce high-speed

pockets in the low-speed flow surrounding the jet, but they are gradually dissipating in the axial direction. In order to reveal the details of the local flow field more clearly, the velocity vectors over a smaller segment of the cross-section is presented in Figure 21. Even here, not every available data point is shown because doing that would make the picture too cluttered, hiding the finer details.

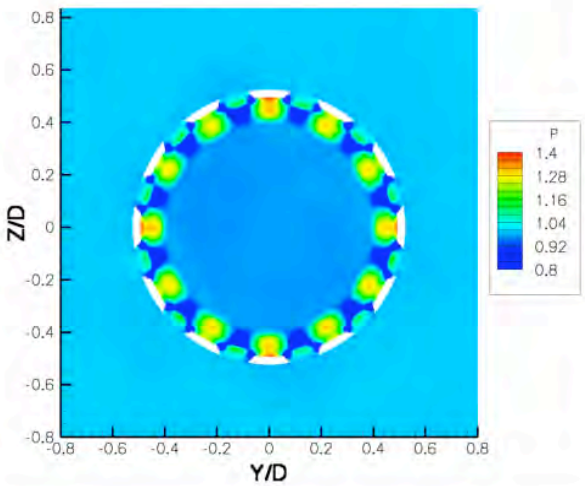

Figure 19. Static pressure distribution at x = 0.1D from a simulation with chevrons.

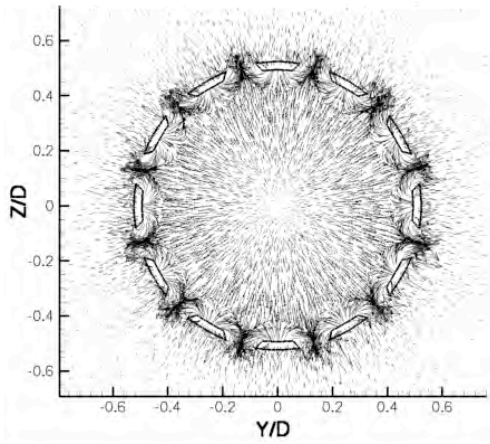

Figure 20. The velocity vector field at x = 0.1D, corresponding to the pressure field shown in Figure 19.

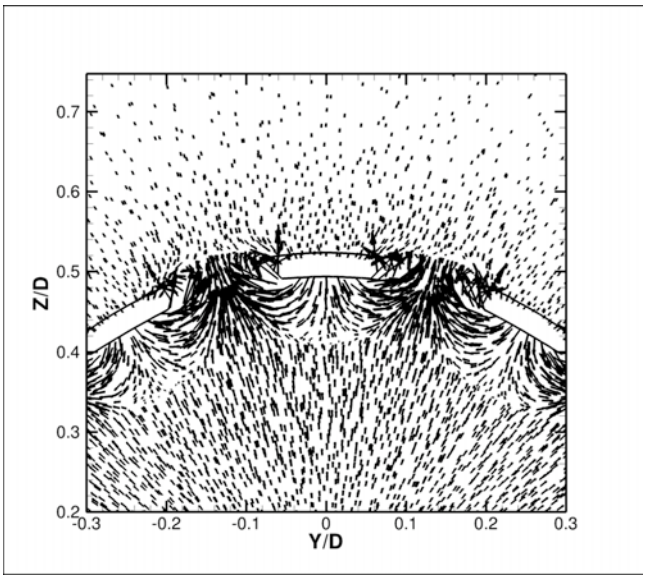

Figure 21. A magnified image showing further details over a smaller segment of the velocity vector field shown in Fig. 20.

The SPL predicted by the simulations with chevrons has been compared to those predicted for the baseline case without chevrons at a series of locations. One such comparison at the near-field location (x = 10.8 D, y = 2.2D) is shown in Figure 22. As shown in this figure (and other data not presented), the screech tone is absent in the simulations with chevrons. Also, there is an overall reduction in the sound pressure levels at other frequencies. The absence of screech was verified experimentally by far-field microphone measurements.

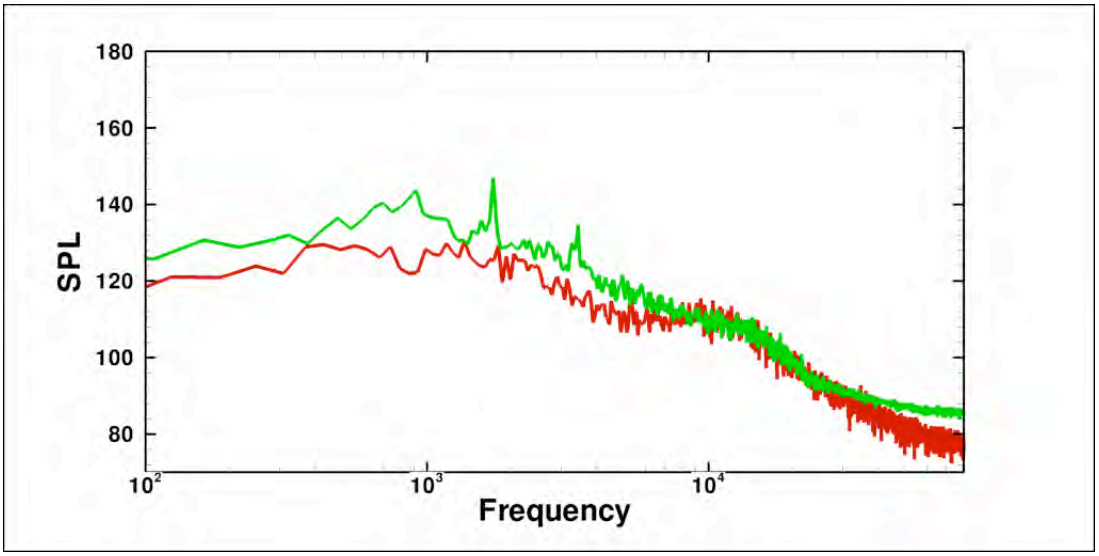

Figure 22. Comparison of the SPL at x = 10.8D, y = 2.2 D predicted by the simulations for the baseline case (green) with those predicted at the same location for the case with mechanical chevrons (red).

In summary**,** these results show that chevrons cause the shock cells to move closer to the nozzle and reduce the spacing between them. In addition, they induce more spread of the jet flow and decrease the strength of the shock cells. All these factors result in a reduction in the noise by more than 3 dB at several locations interrogated. The screech tone, which was so dominant in the baseline nozzle configuration, has been completely eliminated under some conditions or significantly reduced in strength under other conditions.

Impact of Fluidics in combination with Chevrons on Noise Reduction

The next sub-task was to include the impact of fluidic injection (or blowing) on the nozzles with chevrons (as shown schematically in Figure 17). Three flow control approaches were initially screened by far-field acoustic testing. These are: 1) chevrons with a single micro-jet at the tip of each chevron angled at 60° into the flow (12 jets/12 chevrons, Figure 23a), 2) chevrons with two micro-jets on each chevron blowing tangentially along the mid-point of each chevron edge (24 jets/12 chevrons, Figure 28a), 3) micro-jets arranged around a baseline nozzle in place of chevrons (12 jets/no chevrons, Figure 33). The third configuration was for an additional sub-task where we proposed to study the impact of fluidic chevrons (that is, fluidic blowing alone to mimic mechanical chevrons). That is discussed in greater detail in the next sub-section.

Far field measurements showed the 12 jets/12 chevrons configuration to be the best configuration for improving chevron performance. This configuration is shown in Figure 23a. The results in terms of Over All Sound Pressure Level (OASPL) are shown for NPR = 2.5 for two levels of mass flow in Figure 23b. This is the value of NPR for which the chevrons were least effective. The straight black line represents the level of the chevron nozzle. The blue line above it shows the baseline level relative to the chevrons. It can be seen that for this low NPR the chevrons only reduced the OASPL by half a dB in most directions. The application of blowing with 12 jets improved the performance of the chevrons by an additional 1 to 1.5 dB at forward angles and improved the noise somewhat less in the more after directions. This represents a significant improvement in the performance of chevrons at this condition.

The spectral aspects of improvement due to the fluidic injection may be observed in Figure 23c. The left plot is at $\psi = 35°$, the direction in which shock associated noise propagates most strongly. In the baseline case, there is a low screech peak that is slightly higher than the Broadband Shock Associated Noise (BBSN) peak. Chevrons reduce the screech peak slightly, but blowing reduces it to well below the BBSN level. Blowing also reduces the level of the BBSN noise and does not produce high-frequency noise to exceed the baseline case in this direction. The right plot is for an observer at $\psi = 150°$ where the dominant noise source is mixing noise. At lower frequencies the chevrons provide a negligible decrease in sound level while the blowing provides a substantial improvement. At higher frequencies we do see a slight noise increase due to blowing. This high-frequency penalty is typical of chevron behavior, and it can be seen that this extends to blowing as well at the higher microjet mass flow.

There are two approaches to model the fluidic nozzle effects in numerical simulations. One approach is to use numerical inlet boundary conditions to emulate the fluidic blowing, while a second approach is to include the actual fluidic nozzle geometry in the computational domain.

Considering the possible nozzle geometry effects, we have taken the second approach and included the actual fluidic nozzle in the simulations. More set-up work was needed for this approach when compared to the first approach. There were other numerical issues in obtaining the choked flow conditions at the nozzle exit to match the experimental conditions but these were resolved quickly. Simulations were conducted and the results for the various cases were compared with experimental data.

In general both the observations from the experiments and simulations are in agreement though there are some differences due to differing mass flows between experiments and simulations. There was a limit to the mass flow the piping system could supply to the microjets in the experiments. This prevented testing at microjet mass flows as high as those used in the simulations.

A schematic geometry for the 12 jets/12 chevrons configuration is shown in Figure 23a (as mentioned earlier). Numerical simulations show that blowing there induced stream-wise vortices near the nozzle exit (as seen in Fig. 24), but the differences diminish quickly further downstream even by x = 1.0D as shown in Fig. 25 and even further by x = 2.0D as shown in Fig.26. Near-field noise spectra (please see Fig. 27) from the simulations does not show a substantial difference between the two cases in most locations at this under-expanded condition with NPR=4.0. It is found that fluidic injection is less effective at under-expanded conditions. Thus, an over-expanded case should be tested to assess the effectiveness of the combination of chevron and fluidic injection. Hence further studies are recommended.

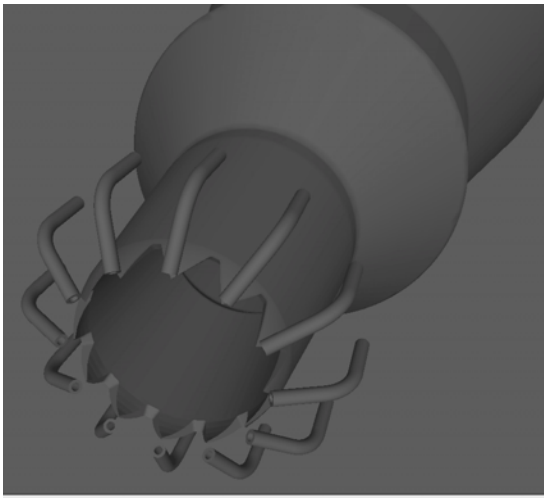

Figure 23a. Geometry of the 12 jet/12 chevron configuration. Each microjet is angled 60° into the main jet at the tip of a chevron.

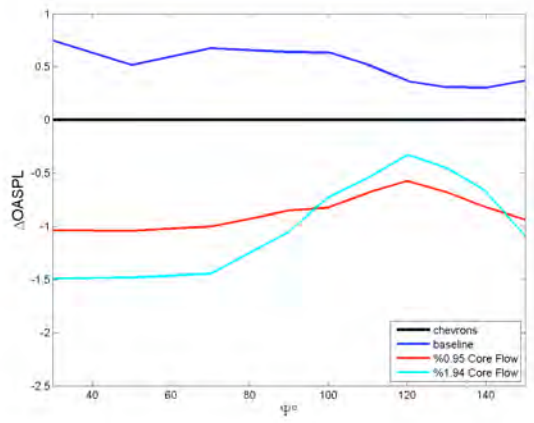

Figure 23b. Overall Sound Pressure Level (OASPL) comparison between baseline (black) chevrons (blue) and blowing 60° at the chevron tips (red and cyan). The ratio of microjet mass flow to core jet mass flow is expressed as a percentage. The core jet NPR is 2.5.

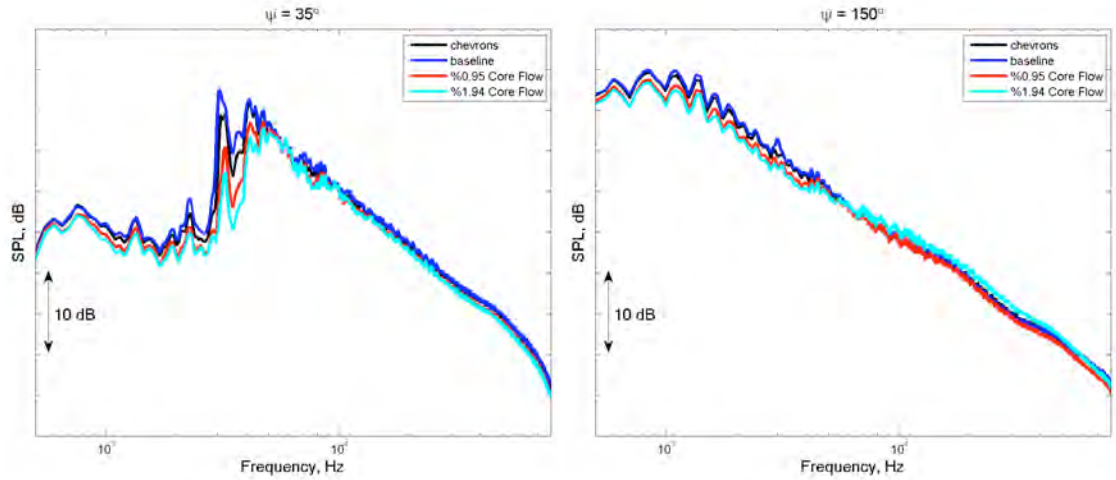

Figure 23c. Sound Pressure Level (SPL) spectra for NPR = 2.5 with and without chevrons and with blowing 60° at the chevron tips at 35° in the forward arc (left) and at 150° in the aft arc (right).

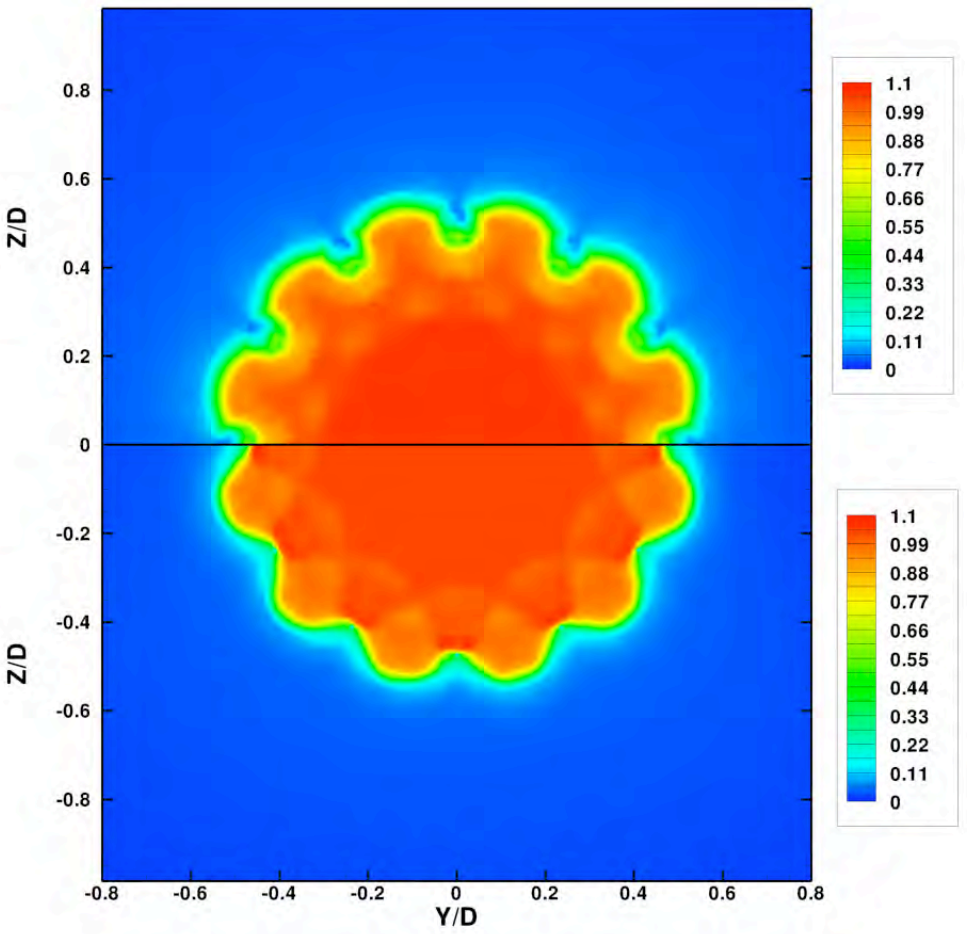

Figure 24. Comparison of streamwise velocity distributions, immediately downstream of main nozzle exit at x=0.2D. Top: 12 jet/12 chevron configuration. Bottom: chevrons alone.

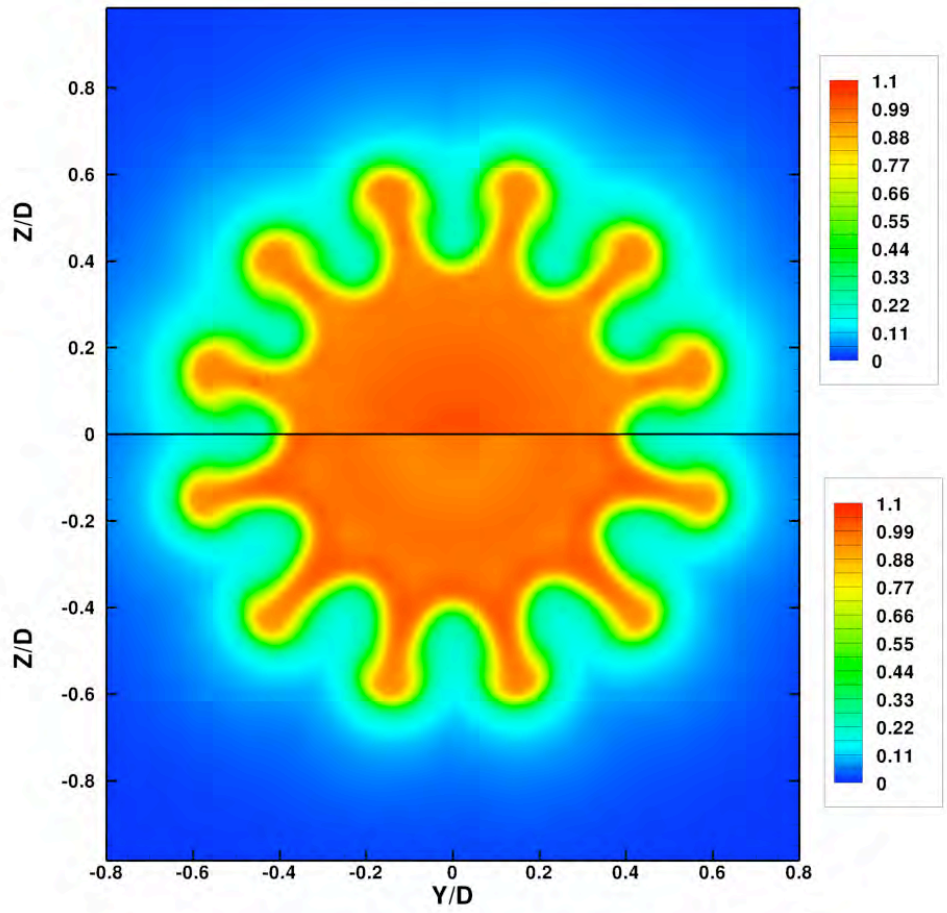

Figure 25. Comparison of stream-wise velocity distributions at x=1.0D. Top: 12 jet/12 chevron configuration. Bottom: chevrons alone without any fluidics.

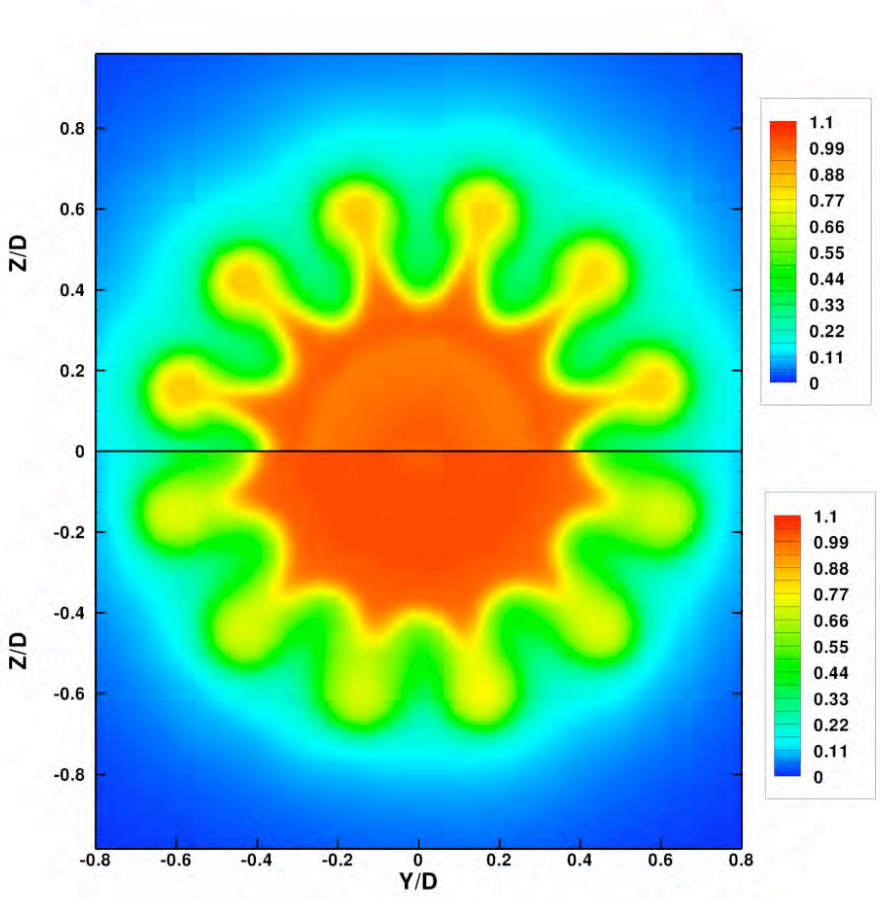

Figure 26. Comparison of stream-wise velocity distributions at x=2.0D. Top: 12 jet/12 chevron configuration. Bottom: chevrons alone without any fluidic nozzles.

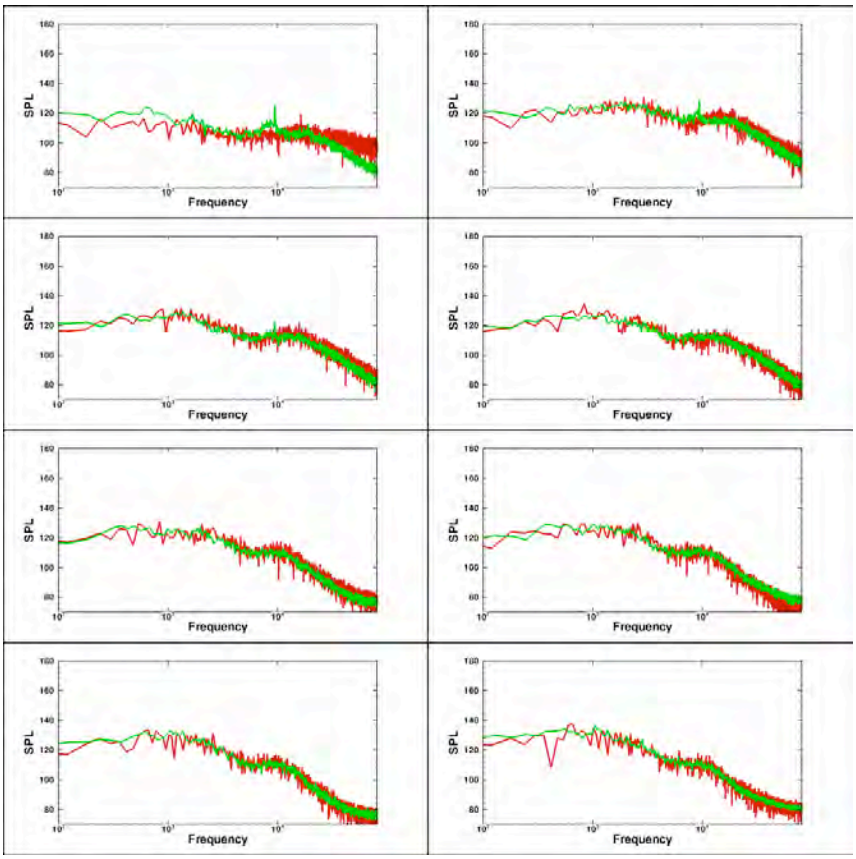

Figure 27. Comparison of noise spectra at eight locations in the jet near-field from numerical simulations. Red: 12 jet/12 chevron configuration. Green: chevrons alone.

The configuration tried next was the 24 jets/12 chevrons configuration, with two microjets per chevron. This geometry is shown in Figure 28a. The microjets are angled 23° toward the axis, which makes them tangent to the outer surface of the chevron at the midpoint between the base and tip. This configuration showed less benefit in the far field. The OASPL for a range of NPR from 2.5 to 5.0 (M_j from 1.22 to 1.71) is shown in Figure 28b. The spectral plots are shown in Figure 28c. The blowing in this configuration did not produce appreciable improvement in the far field. Since the limited mass flow was divided among 24 microjets, and since the unlimited mass flow in the simulations showed better results than the experiments we believe that further investigation is warranted with greater mass flow to the microjets.

The LES applied larger mass flows through the microjets and obtained better results. Figure 29 shows the stream-wise velocity distributions for both cases: chevrons alone and the 24 jets/12chevrons configuration. It can be seen from the figure that fluidic injection increases the area of high-speed fluid. The vector fields shown in Fig. 30 indicate that fluidic injection generates another pair of counter-rotating vortices in addition to the one generated by chevrons. However, at more downstream locations, those two pairs coalesce into one pair. But at x = 2D, (as shown in Fig. 31), the strength of the high-fluid area is much stronger in the case with fluidic injection when compared to the case with just the mechanical chevrons. The noise spectra from the simulations are shown in Fig. 32 for eight locations. The case with the chevrons in

combination with fluidic injection shows a slightly lower magnitude near the nozzle exit but overall the two spectra do not show any dramatic differences. Again, modifying the injection angle and other parameters could show bigger differences.

Fluidically enhanced chevrons were shown both in subsonic and supersonic jets to be effective in increasing the noise reduction by chevrons by a factor of 2-3. The mechanism by which the method works depends on the location of injection. When the microjets are placed at the chevron tips, they produce additional streamwise vortices. When they are placed along the slanted sides of the chevrons, in addition to generating additional streamwise vortices, they energize the vortices produced by the chevrons and prevent their breakdown. However, effective generation of streamwise vorticity and energizing the chevron vortices are highly sensitive to several parameters: microjets momentum, velocity, injection angles (yaw and pitch), location, and microjet tube size. This high sensitivity can explain the difference between the results obtained experimentally and through CFD. The latter added crucial information for the understanding of the physical mechanism of this method. Optimization of each one of these parameters is required to achieve best performance.

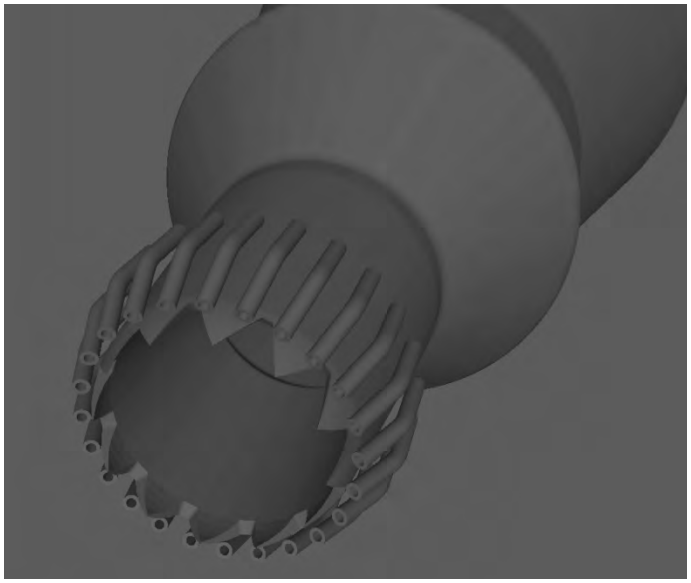

Figure 28a. Fluidic Geometry of the 24 jet/12 chevron configuration. Each microjet is angled 23° into the main jet which is tangent to the outside of the chevron at the chevron edge's midpoint.

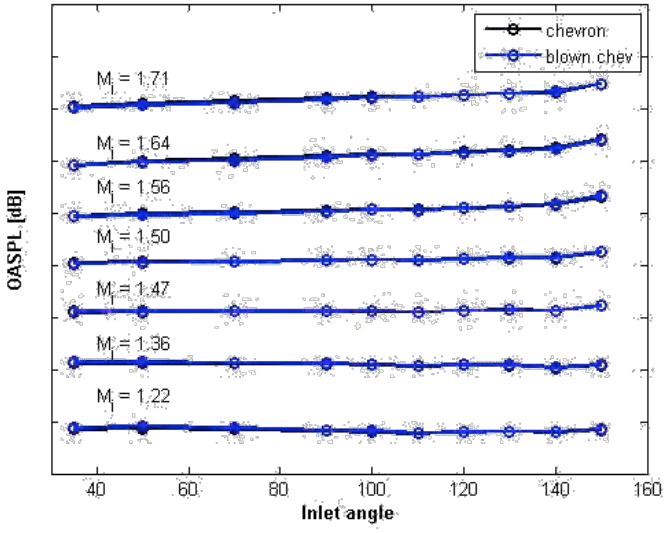

Figure 28b. Overall Sound Pressure Level (OASPL) chevron (black) and 24 jet/12 chevron configuration (blue).

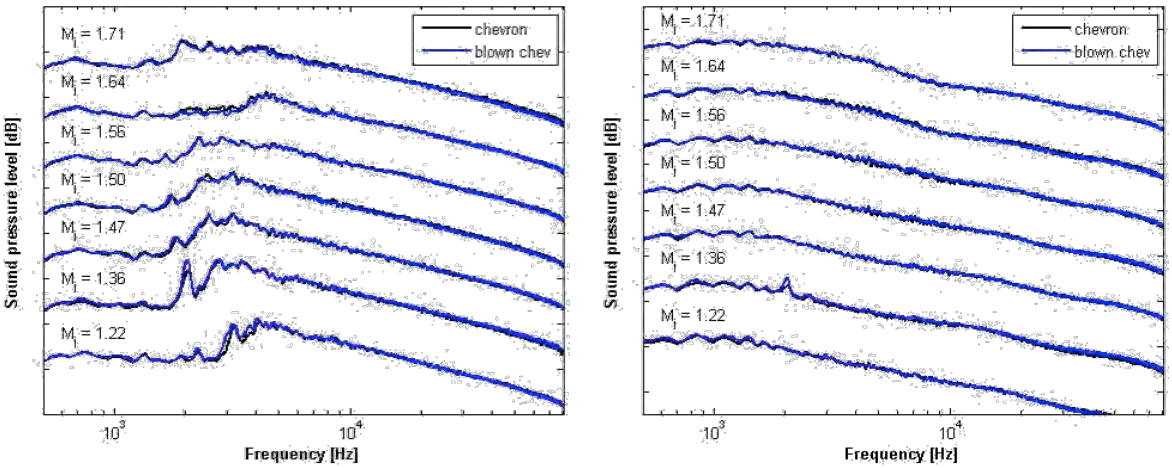

Figure 28c. Sound Pressure Level (SPL) spectra with and without chevrons and with 24 jet/12 chevron configuration in the forward arc (left) and at 150° in the aft arc (right).

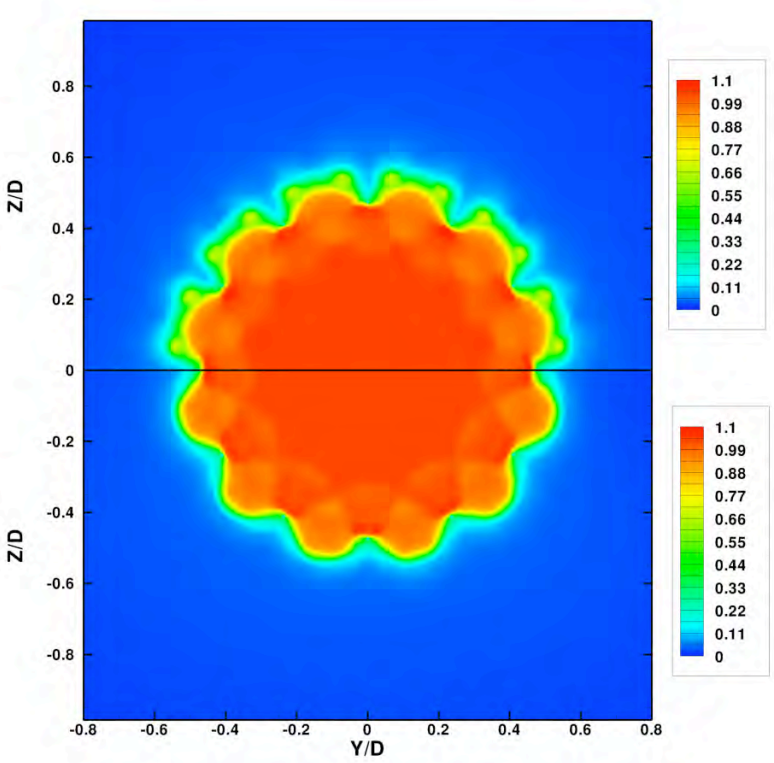

Figure 29. The comparison of stream-wise velocity distributions at x=0.2D, immediately downstream of main nozzle exit. Top: 24 jet/12 chevron configuration. Bottom: chevrons alone.

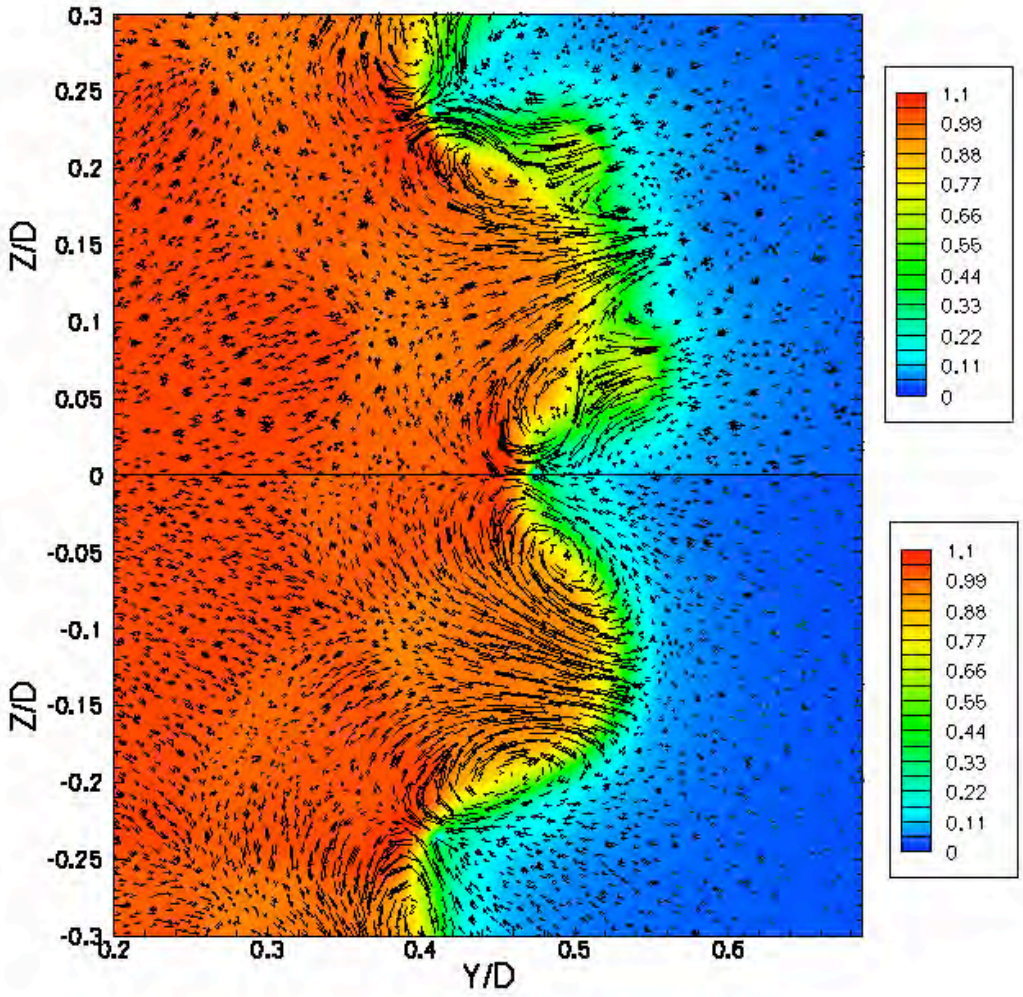

Figure 30. The comparison of stream-wise velocity distributions overlaid with vector fields at x=0.2D, immediately downstream of main jet nozzle. Top: 24 jet/12 chevron configuration. Bottom: chevrons alone.

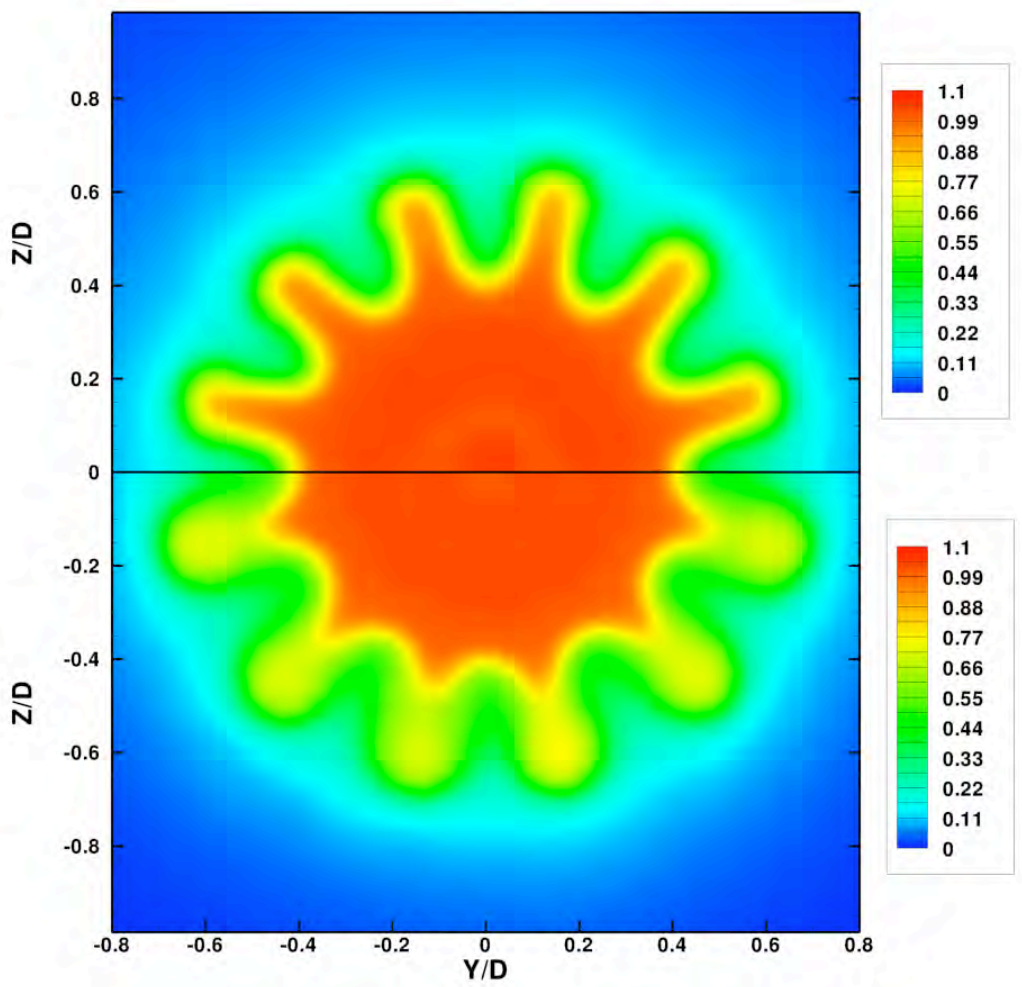

Figure 31. The comparison of stream-wise velocity distributions at x=2.0D. Top: 24 jet/12 chevron configuration. Bottom: chevrons alone.

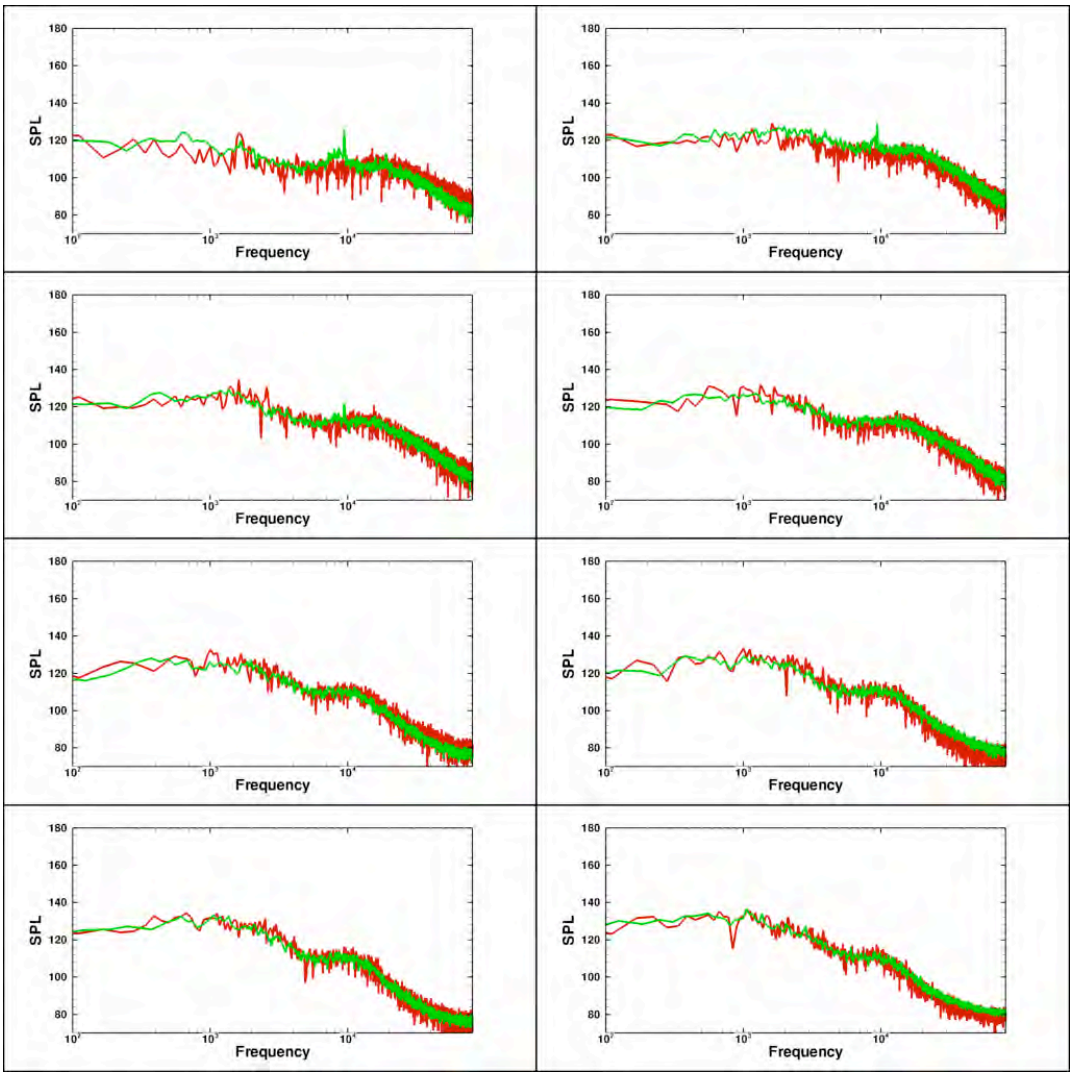

Figure 32. Comparison of noise spectra at eight locations from numerical simulations. Red: 24 jet/12 chevron configuration. Green: chevrons alone.

Impact of Fluidic Chevrons (Fluidic jet replacement of mechanical chevrons)

The next sub-task on noise reduction techniques was investigation of the effectiveness of fluidic injection alone, without any mechanical chevrons. Practically, this could be important because fluidic injection can be turned on and off as needed while the mechanical chevrons are always physically present once installed on the engine nozzle. Since mechanical chevrons have adverse effect on the engine performance (reduced thrust) throughout the entire flight while noise reduction is needed primarily during take-off, the ability to turn them on only when needed is very important. So this technique can also be called as “fluidic chevrons”, as opposed to mechanical chevrons.

First we discuss the case with twelve injection nozzles, each at a 60 degree injection angle (the 12 jets/no chevrons configuration). This is parallel to the 12 jets/12 chevrons

configuration discussed above but now the baseline nozzle is used without any mechanical chevrons. Figure 33a shows the fluidic injection configuration with twelve evenly distributed micro jets for fluidic injection. The micro jets have a slightly convergent section at the end and the diameter is 0.12". The injection angle for this case is 60^{o}. For the numerical simulations, tetrahedral meshes were used to model the whole geometry and fine grid cells were clustered around the nozzle exit and micro-jet geometries. Since the primary nozzle lip thickness is only 0.02", which is 1.5 times smaller than the finest grid size used, the impact of lip thickness is not considered in this study.

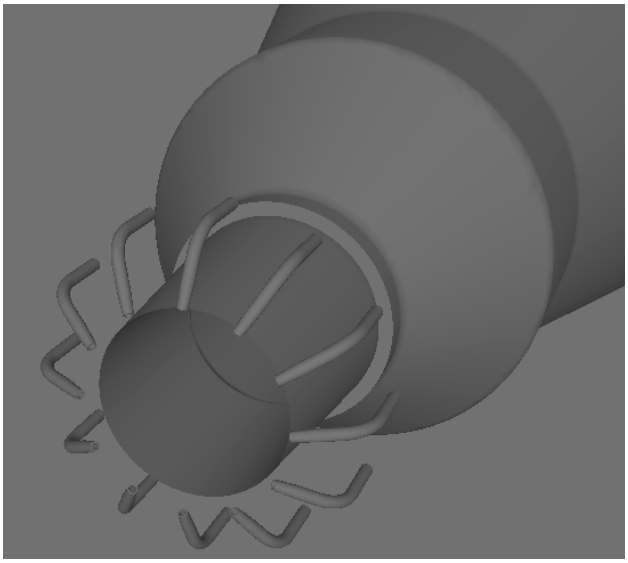

Figure 33a. Nozzle Geometry of the 12 jet/no chevron configuration. Each microjet is angled 60° into the main jet.

The far-field results are shown in Figure 33b for the OASPL and Figure 33c for the spectral results. Three nozzle pressure ratios are shown. NPR = 2.5 (M_j = 1.22) is an overexpanded case in which the blowing was quite effective, with 1% microjet mass flow producing improvements of 3 dB in the forward arc and around 1.5 dB in the aft arc at 130°. The on-design case, NPR = 3.671, M_j = 1.5 shows less reduction. This is likely due to a lower mass flow percentage as the main jet mass flow was increased while the microjets remained at the upper limit imposed by the supply piping. The highest case, NPR = 5.0, M_j = 1.71 shows the least improvement since at this elevated jet mass flow the microjets could only supply 0.5% of the main jet's mass flow.

The simulations faced no limit on the mass flow to the microjets. The nozzle pressure ratios of micro jets were set to the same value as that of the primary jet. The mass flow rate of injected air by the twelve micro jets is around 2.2% of the mass flow rate from the primary jet. Since it was found that the chevron nozzle is effective in eliminating screech tones and reducing both broadband shock-associated noise and mixing noise, results of fluidic injection are compared with those produced by the chevron nozzle to measure the relative effectiveness of fluid injection.

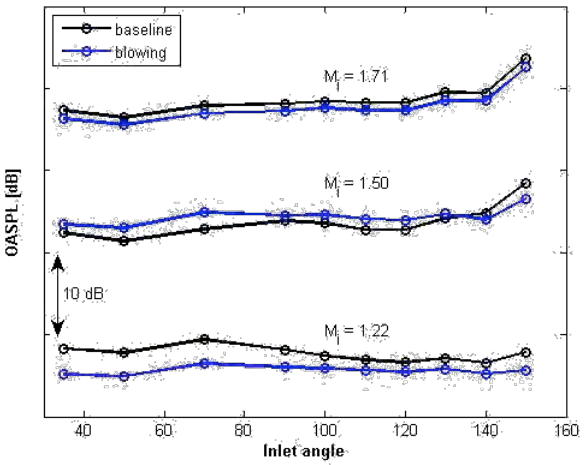

Figure 33b. Overall Sound Pressure Level (OASPL) baseline (black) and 12 jet/no chevron configuration (blue).

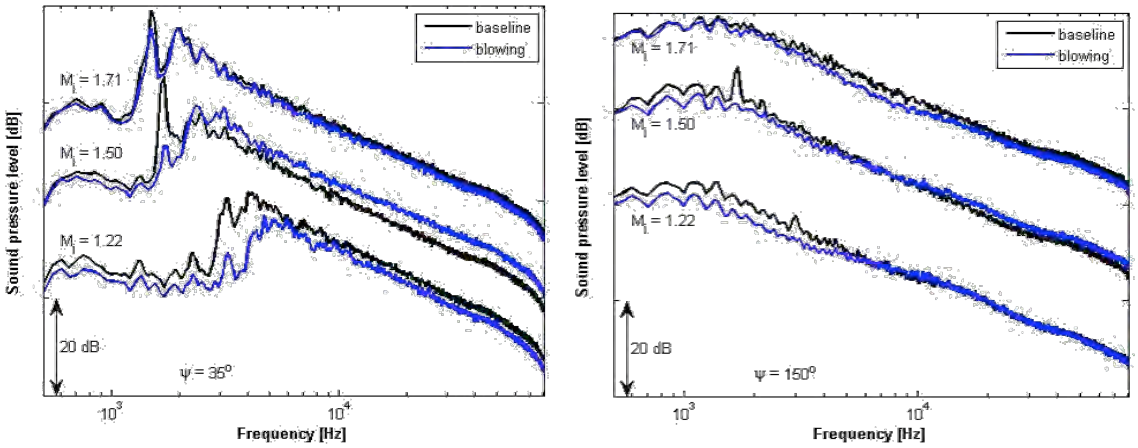

Figure 33c. Sound Pressure Level (SPL) spectra for the baseline nozzle and with 12 jet/no chevron configuration for an observer at 35° in the forward arc (left) and at 150° in the aft arc (right).

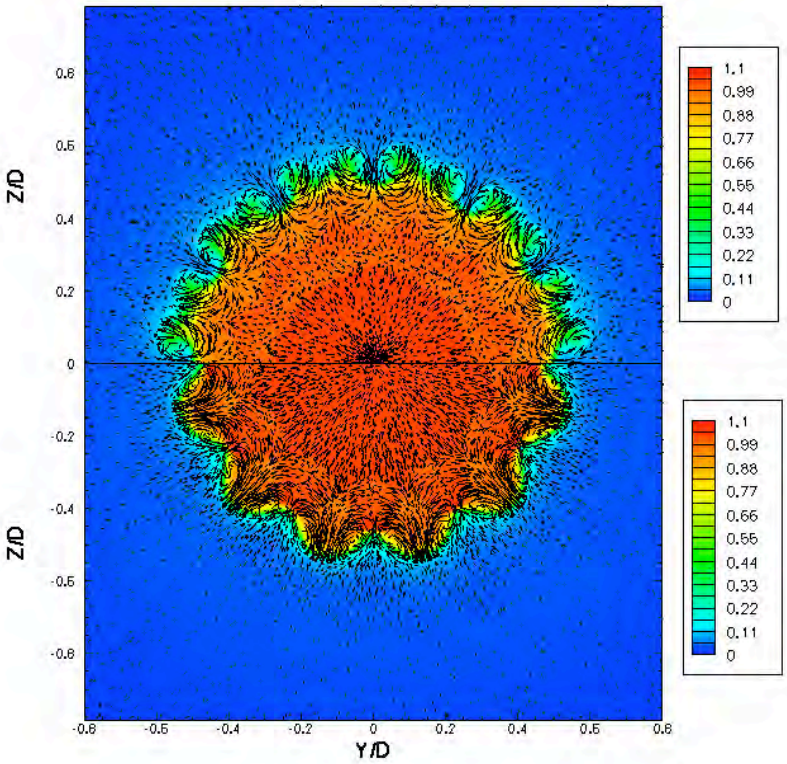

Figure 34. Velocity vector field overlaid with the stream-wise velocity at x = 0.2D. Top half of figure: 12 jet/no chevron configuration. Bottom half of figure: chevron nozzle.

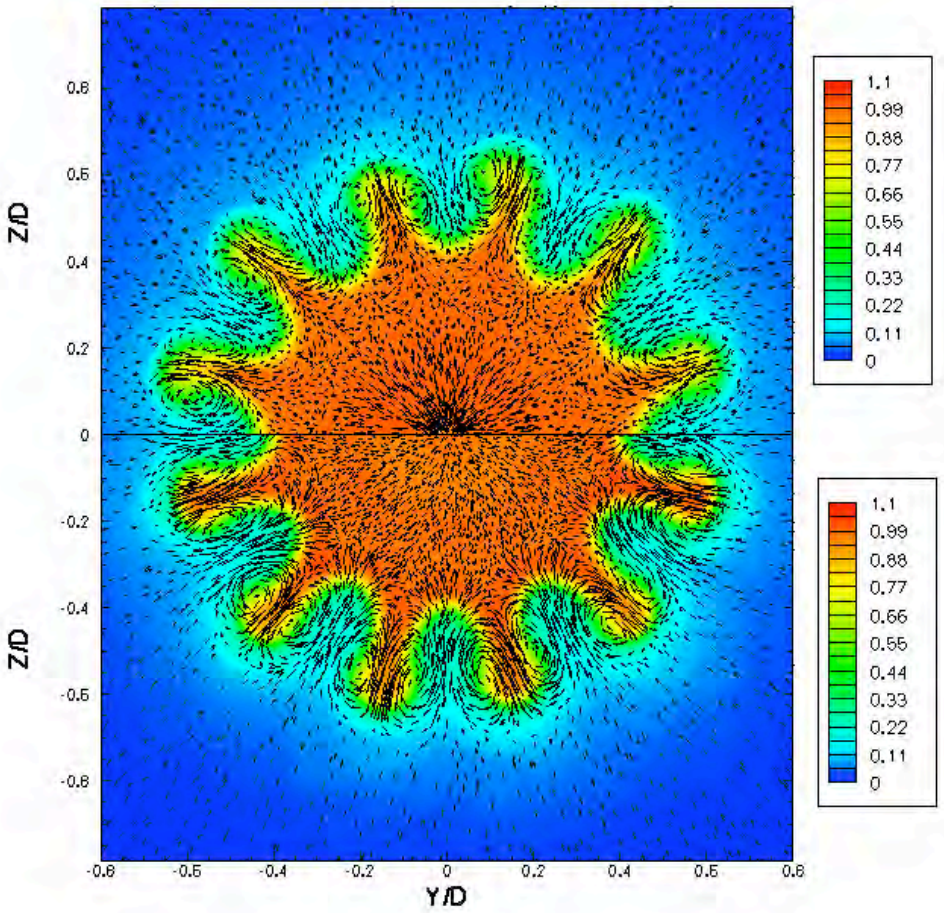

Figure 35. Velocity vector field overlaid with the stream-wise velocity at x = 1.0D. Top half: fluidic 12 jet/no chevron configuration. Bottom half: chevron nozzle.

Figures 34 and 35 show the cross stream velocity vector field of the 12 jets/no chevrons configuration at x = 0.2D, just slightly downstream of the main nozzle exit and at x = 1.0D, further downstream, along with those produced by the chevron nozzle. It can be seen that fluidic injection forms counter-rotating vortices similar to those produced by the chevron nozzle.

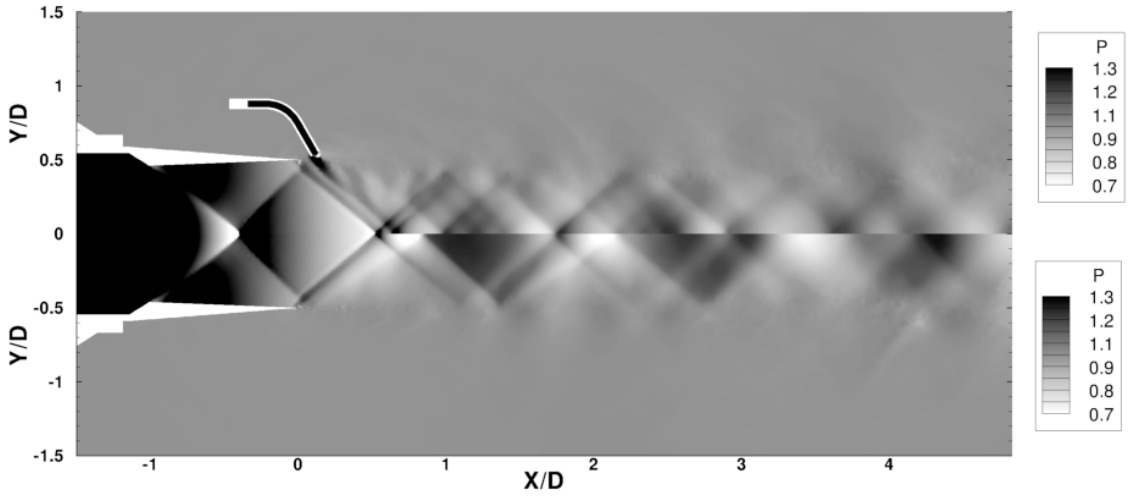

Figure 36. Comparison of static pressures for the 12 jet/no chevron configuration (top half) against baseline nozzle case (bottom half).

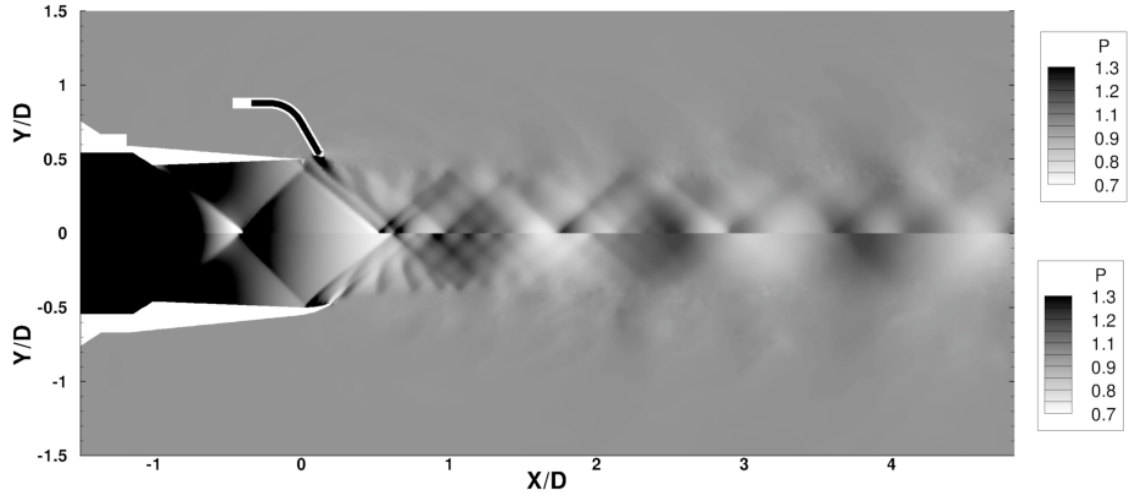

Figure 37. Comparison of static pressures for the 12 jet/no chevron configuration (top half) against the equivalent chevron nozzle case (bottom half).

Figures 36 and 37 compare the static pressure flow field (highlighting shock-cell distributions) produced by the baseline nozzle, the nozzle with fluidic injection alone and the chevron nozzle case. It is found that fluidic injection modifies the shock-cell structures and weakens the shock-cell strength. It also introduces pressure disturbances with small wavelengths near the nozzle exit, similar to what the chevron nozzle has produced.

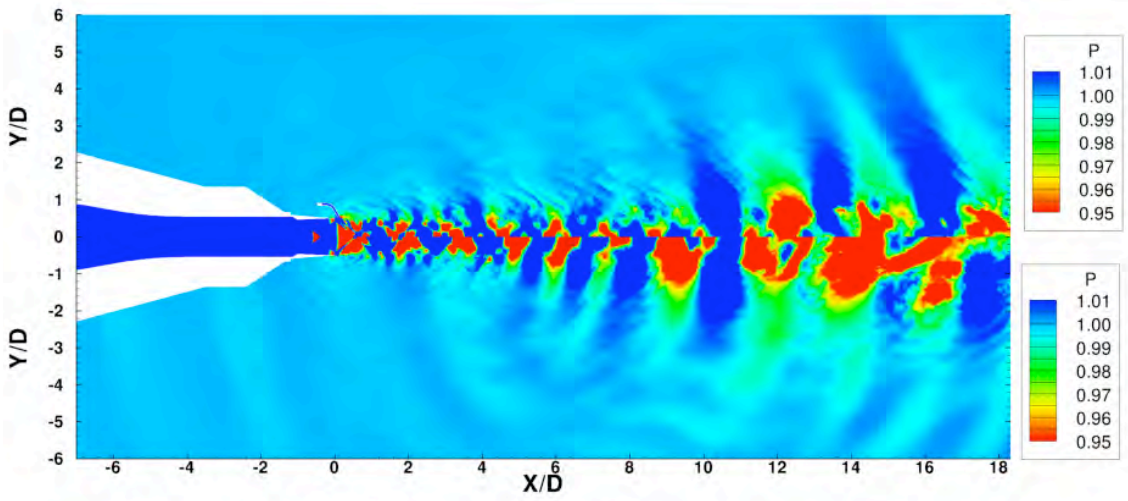

Figure 38. Instantaneous non-dimensional static pressure distributions from: Top half: 12 jet/no chevron configuration; Bottom half: baseline nozzle case.

Figure 38 shows the instantaneous pressure distributions from both the baseline nozzle case and from the nozzle with the 12 jets/no chevrons configuration. The contour levels selected are near the acoustic range to display turbulence structures that could be associated with noise-generation. It can be seen that large-scale turbulence structures are reduced significantly with fluidic injection when compared with those from the baseline nozzle. Therefore, the streamwise vortices do suppress the formation of the large-scale turbulence structures and consequently it would be expected that fluidic injection would reduce the turbulence intensity and noise levels.

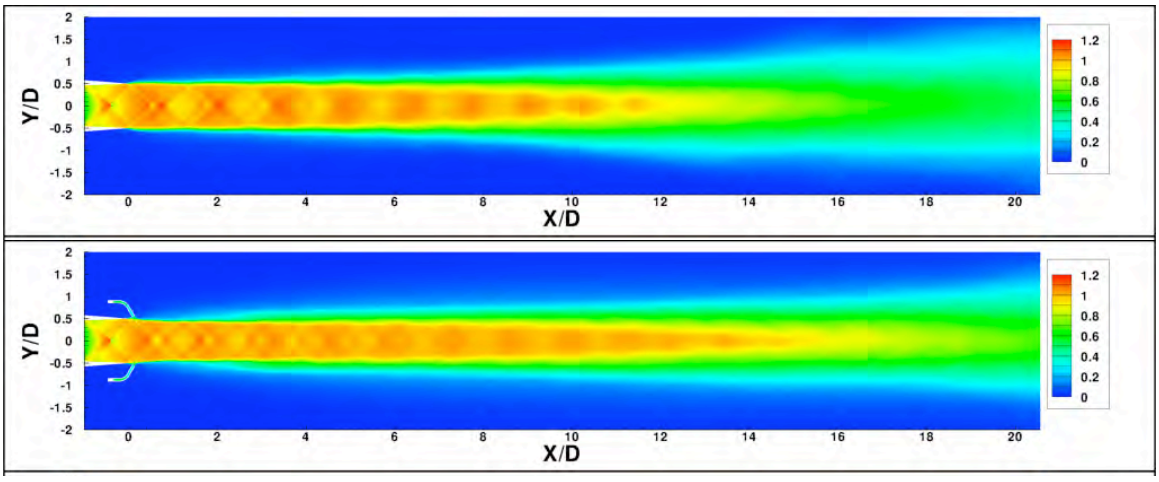

Figure 39. Stream-wise velocity distributions. Top: baseline C-D nozzle case. Bottom: 12 jet/no chevron configuration.

The streamwise velocity distributions for both the baseline nozzle and the nozzle with fluidic injection are shown in Fig. 39. It is observed that fluidic injection increases slightly the jet core length. This phenomenon was also observed in previous experimental work on supersonic twin jets by Alkislar et al. [32]. It is suggested that although the streamwise vortices initially increase mixing and increase the shear-layer thickness near the nozzle exit, they reduce the shear-layer spreading because of the suppression of the large-scale turbulence structures and slow the break down of the jet core. Figure 40 shows the turbulent kinetic energy distributions from the simulations of both the baseline nozzle and the nozzle with fluidic injection. As would be expected the turbulence kinetic energy is reduced and the high-turbulence region is pushed further downstream for the case with fluidic injection.

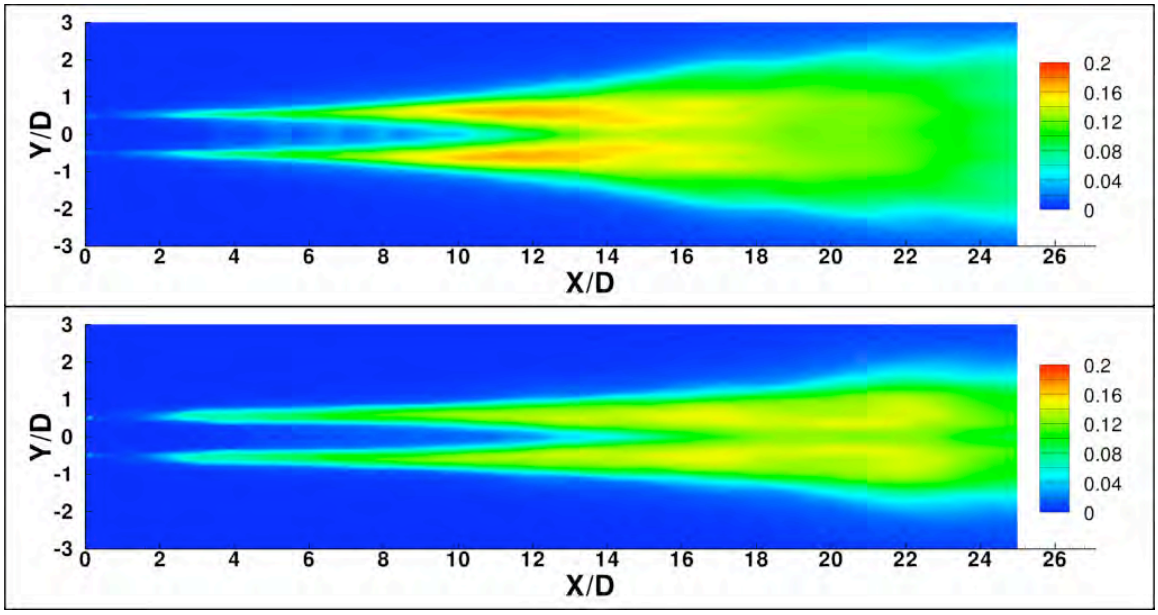

Figure 40. Computed turbulent kinetic energy distributions from both the baseline nozzle and the nozzle with fluidic injection. Top: baseline nozzle. Bottom: nozzle with fluidic injection.

Figure 41 shows the noise spectra at three near-field locations from the numerical simulations. The first two of them are in the region where most of the shock-associated noise is generated and the third location is in the mixing region. The noise spectra of the baseline nozzle and those of the chevron nozzle are also shown in each figure to compare with those from the fluidic injection case. The noise modification due to pure fluidic injection is similar to that of the chevron nozzle and significant noise reduction is seen in the region dominated by shock-associated noise. Fluidic injection increases the high-frequency noise slightly near the nozzle exit when compared to the baseline nozzle.

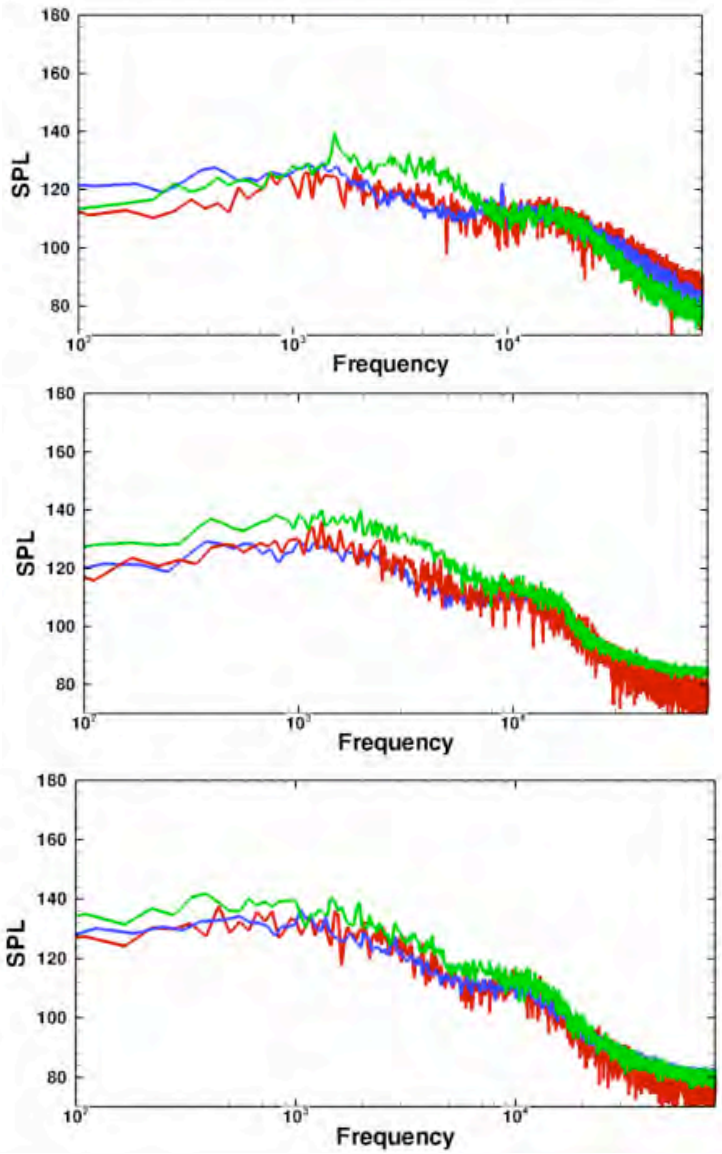

Figure 41. The computed noise spectra at three locations. Top: x = 4.4D, y = 1.4D. Middle: x = 10.8D and y = 2.2D. Bottom: x = 15D and y = 2.6D. Green lines: baseline nozzle. Red lines: 12 jets/no chevrons. Blue lines: chevron nozzle.

With the promise shown by purely fluidic injection (in place of mechanical chevrons), additional cases were studied including varying the number of micro-jet injection nozzles from 12 to 16 and the injection angle to higher values up to 90 degrees.

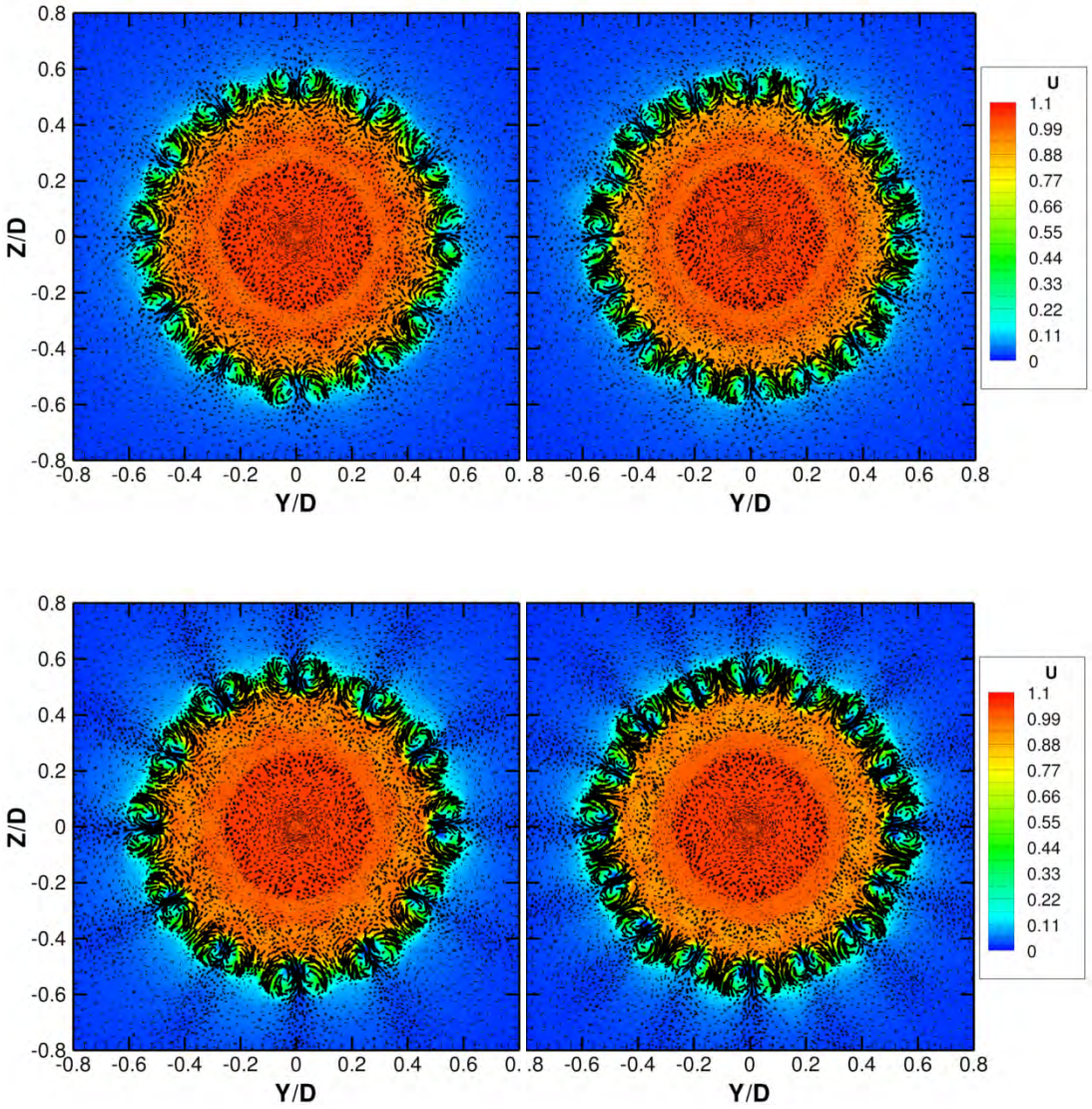

Figure 42. Vector fields from simulations of four configurations at x=0.2D, immediately downstream of the micro jets. The four configurations are: 1) 12 nozzles at 60 degrees (upper left), 2) 16 nozzles at 60 degrees (upper right), 3) 12 nozzles at 90 degrees (lower left) and 4) 16 nozzles at 90 degrees (lower right).

Figure 42 compares the vector fields of four injection conditions at a location immediately downstream of the nozzle exit. Injection at 90^o gives stronger vortices. Further downstream at x = 2D as shown in Fig. 43, vortices generated by 16 nozzles dissipates faster, probably because the vortices stay closer and interact with each other. The vortices generated by 60^o and 90^o are similar to each other at this location.

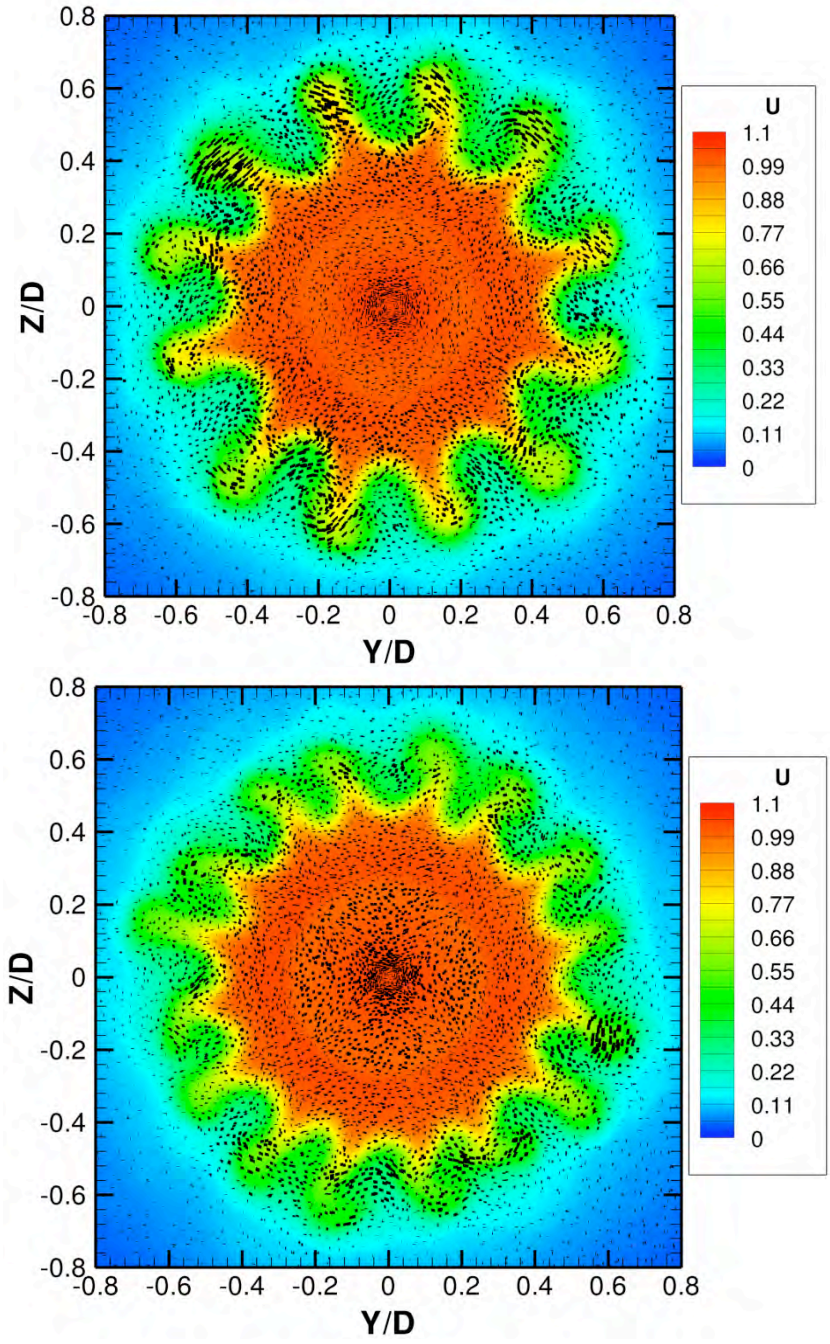

Figure 43. Vector fields at x = 2D. Top: 12 nozzles at 60°. Bottom: 16 nozzles at 60°.

Figure 44 shows the density distributions for all four cases, along with those from the baseline nozzle and chevron nozzle. Fluidic injection re-enforces the waves generated by the nozzle lip and generates high-pressure spot in the core. The strength of the high pressure in the jet core increases with injection strength. Figure 45 shows the noise spectra for the four injection conditions at three locations. The difference between the cases is small. However, it seems that the configuration of 12 nozzles at 90° damps more high-frequency information near the nozzle

exit, but increases more low-frequency components. Overall, it seems the configuration of 16 nozzles at 90^{o} shows a slightly better performance.

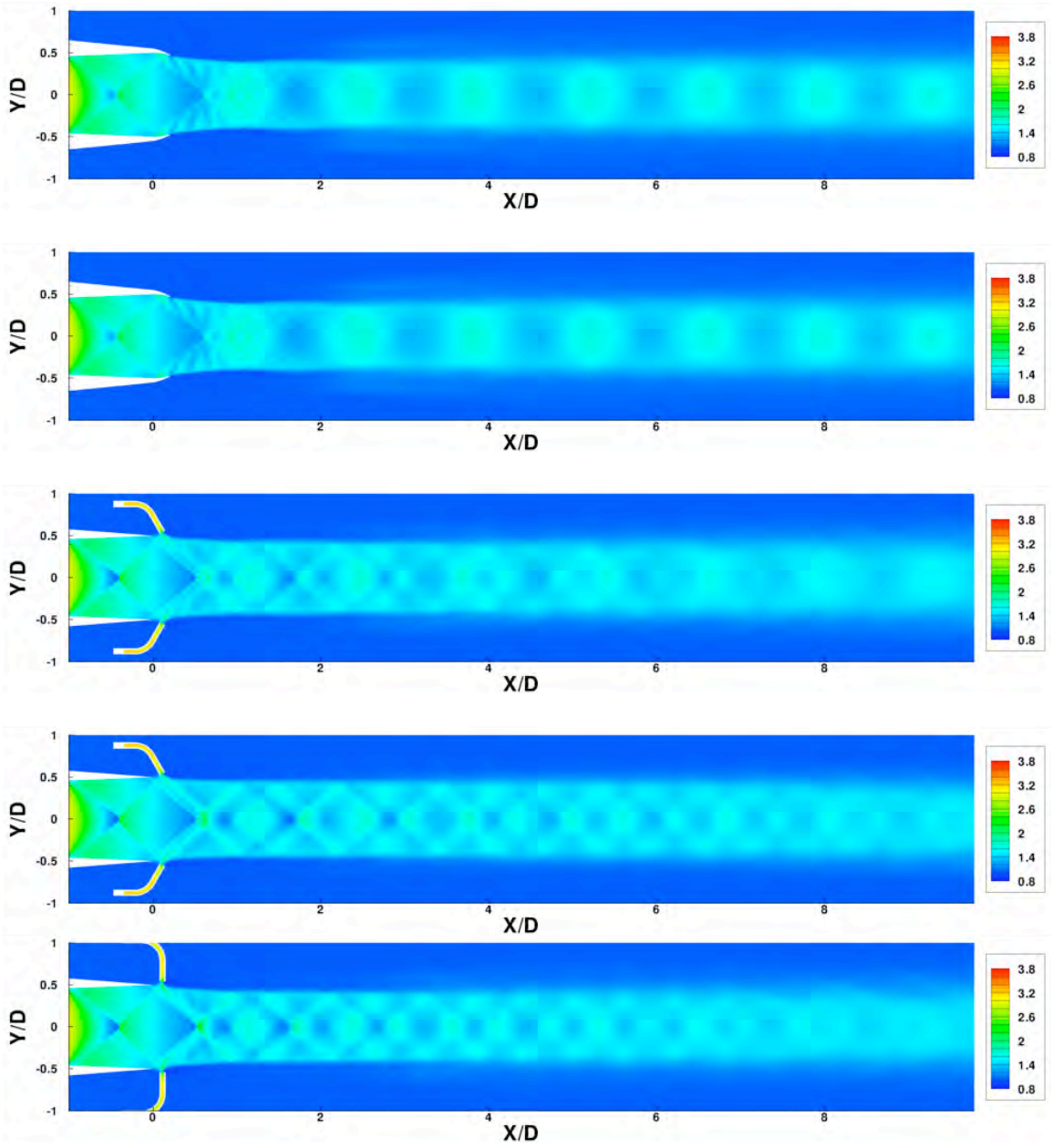

Figure 44. Density distributions (scaled by the ambient condition) for the chevron nozzle case (topmost) and the four fluidic-injection configurations (12 nozzles at 60^{o}, 16 nozzles at 60^{o,} 12 nozzles at 90^{o}, 16 nozzles at 90^{o} (from top to bottom after the chevron case).

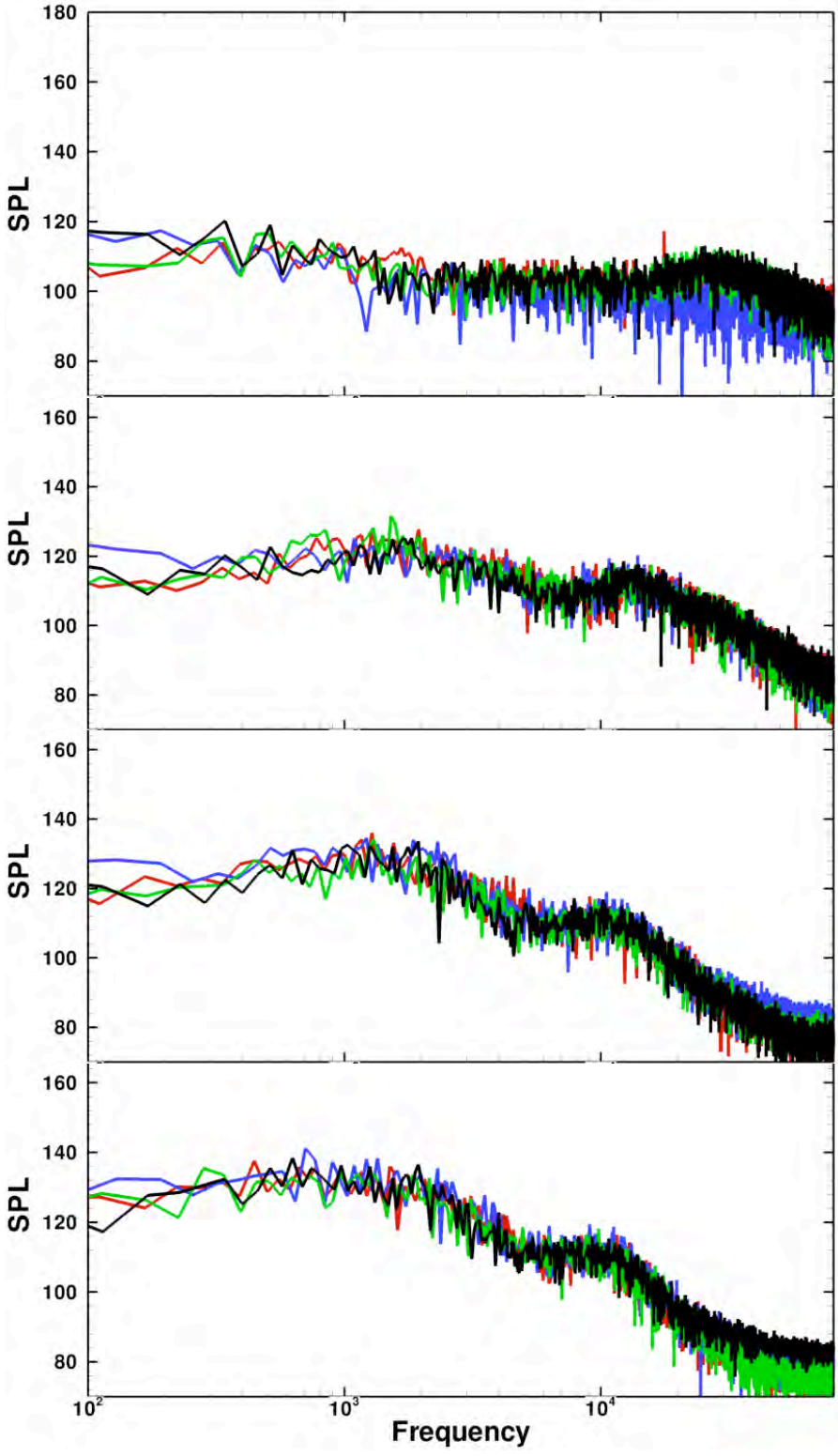

Figure 45. Noise spectra at several locations for the four configurations. Red: 12 nozzles at 60°. Green: 16 nozzles at 60°. Blue: 12 nozzles at 90°. Black: 16 nozzles at 90°.

Summary of Observations on Fluidic Injection and Chevrons:

In summary, the studies with fluidic injection show that fluidic injection enhances mixing and increases the shear-layer thickness near the nozzle exit. Fluidic injection also suppresses the growth of large-scale coherent structures and results in a reduced growth rate of the shear-layer thickness further downstream of the nozzle; an increase in the potential core length; reduced turbulence levels and reduced noise intensities, especially in the region where shock-associated broadband noise is dominant. Fluidic injection also modifies the shock-cell structure, reducing the shock strength. However, as with mechanical chevrons, high-frequency components near the nozzle exit are strengthened (increased). In general, fluidic injection in place of mechanical chevrons shows promise. For a constant injection mass flow, the effectiveness of fluidic injection decreases with increasing jet Mach number. Fluidic injection in combination with mechanical chevrons, in general, enhances the chevron effectiveness, especially at low values of jet Mach number. As reported previously, these are the Mach numbers where chevrons alone tend to be less effective. **So fluidic injection does provide a complementary technique to mechanical chevrons for noise reduction**.

Fluidic Injection for Area-Ratio Control

The final noise reduction strategy planned for investigation was using fluidics to effectively modify the area-ratio of the nozzle. The idea is that, moving the effective operating conditions towards the nominally ideally expanded conditions, will result in weaker shocks and consequently, lower levels of shock associated noise. The arrangement used was to blow air from an annular slot in the divergent section of the nozzle to influence the effective area ratio (ratio of area of the throat of the nozzle to the exit area) of the nozzle as an alternative to changing the physical area ratio, or in order to enhance the match between the design Mach number (depends directly on area ratio) of the nozzle and the jet Mach number (depends directly on pressure ratio.) The slot in the divergent section of the nozzle is 1/3 of the way from the throat of the nozzle to the exit. A schematic of the system used is shown in Fig. 46 with the injection path highlighted in red. Aside from the slot the internal flow lines match those of the previously tested $M_d = 1.5$ baseline nozzle against which results are compared. Both experiments and three-dimensional numerical simulation were conducted.

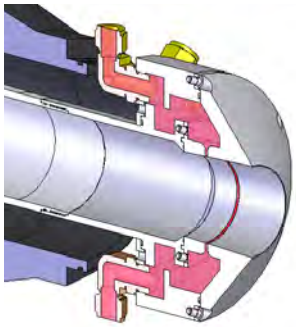

Figure 46. Schematic of the system used for annular fluidic injection to vary the effective area-ratio.

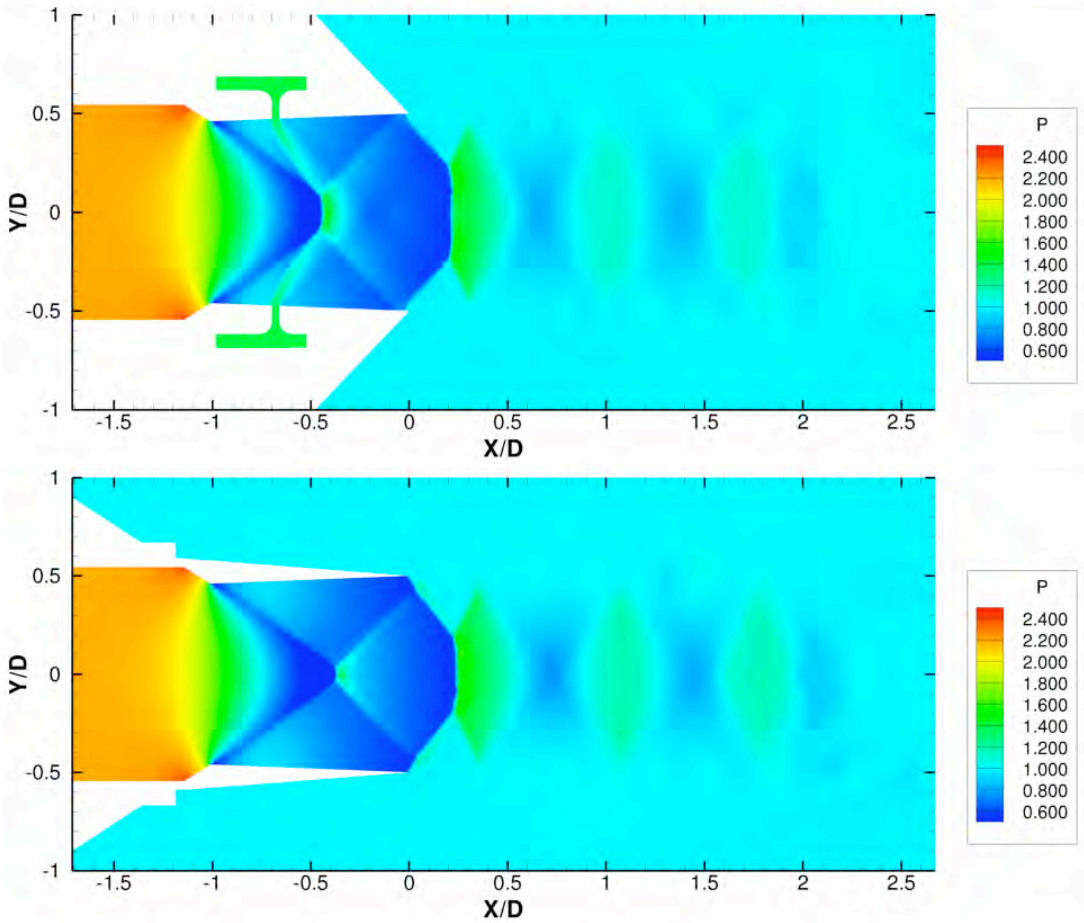

Figure 47. Static pressure distribution (P/P_∞) of a C-D nozzle with annular fluidic injection for the case with NPR = 2.5. The injection flow rate is zero for this case. The figure at the bottom is the baseline nozzle without the injection set-up, for reference in comparison discussions.

The initial focus was on an over-expanded jet case with NPR = 2.5. It is found that the injection pressure for this NPR has to be greater than 1.393 P_∞ to have a positive injection velocity. Otherwise, the flow will be reversed and will flow into the injection chamber from the main nozzle. The simulations show that the very presence of the injection slot (even with zero mass inflow rate) has an impact on the shock-cell structures. The static pressure distribution for this case is shown in Fig. 47. The higher static pressure inside the injection chamber emanates a high-pressure wave, producing a larger buildup of high pressure at the center. This high-pressure region produces a compression wave slightly more upstream than what is observed in the baseline C-D nozzle case (also shown for reference in Figure 47). Other simulations with higher injection mass flow rates show (Fig. 48) that the area of the high-pressure region increases as the mass flow rate increases. Some more compression and expansion waves occur until the injection flow rate reaches a certain critical value when the expansion wave induced by the physically sharp throat is completely overshadowed by the wave system set up by the fluidic injection. For this NPR, this critical mass flow rate is 8.8% of the main jet mass flow rate. For this relatively large injection mass flow rate, the effective throat location has moved downstream, slightly behind the injection location. Hence, the shock cell structure is also altered which in turn should

alter the generation of noise. Further analysis of the static pressure distributions at the nozzle exit indicate that as the injection flow rate increases, the static pressure also increases. For example, with a relatively modest injection mass flow rate of 2.17%, the flow is less over-expanded at the nozzle exit than the baseline case. This is the effect we hypothesized originally and further analysis shows a beneficial noise reduction.

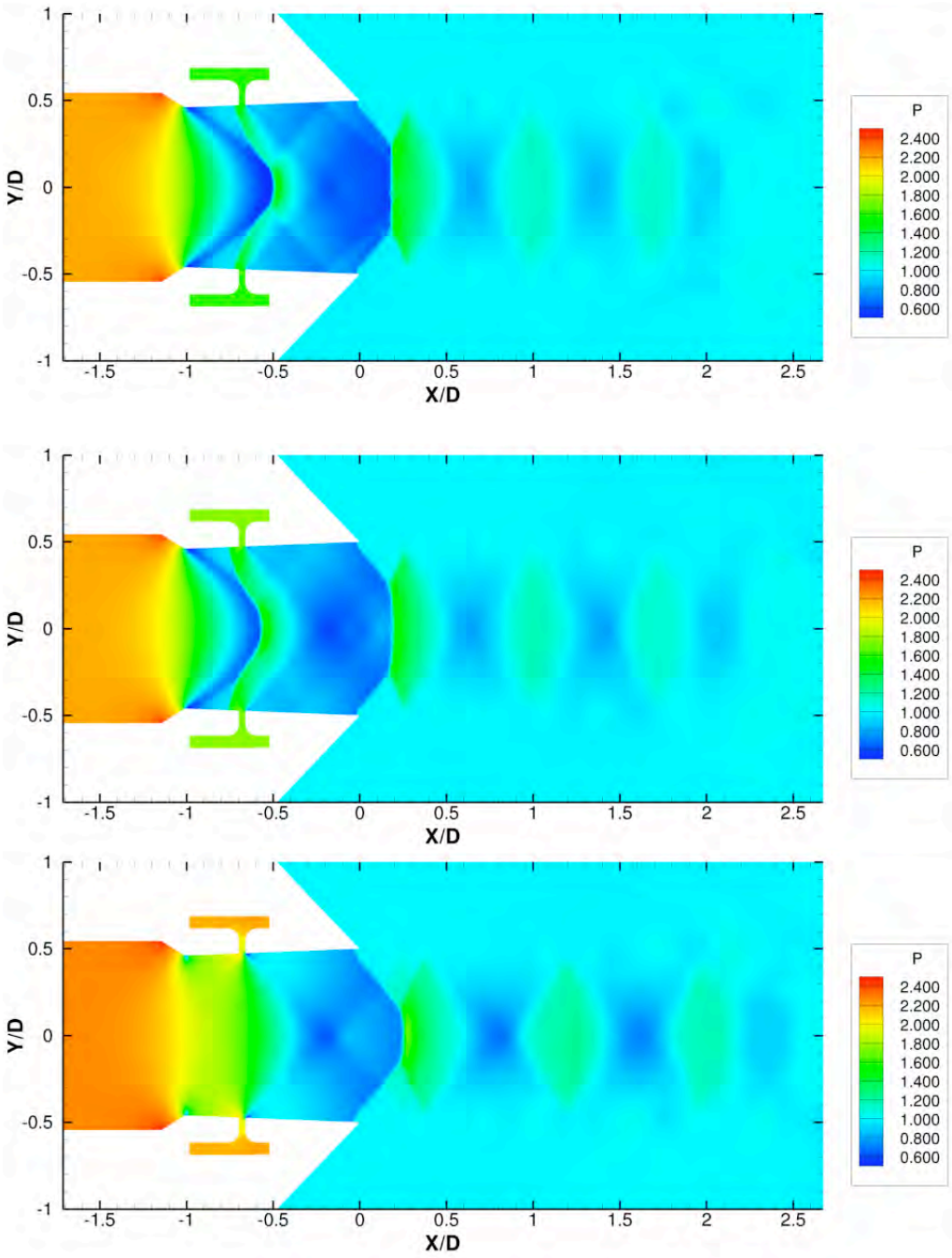

Figure 48. Static pressure distributions with three injection mass flow rates. Top: 1.06%. Middle: 2.17%. Bottom: 8.80%.

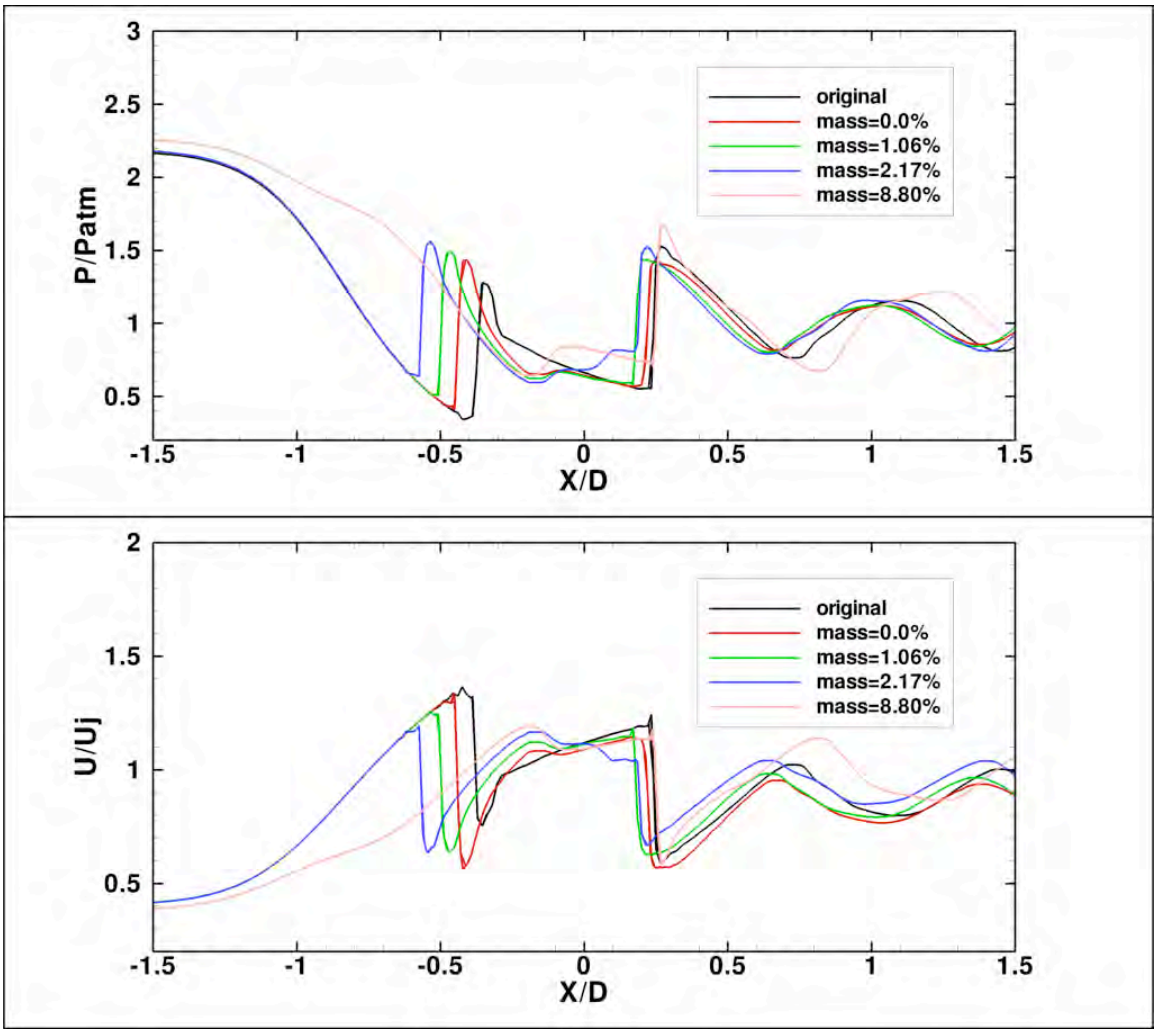

Figure 49. Static pressure and velocity distributions for both the baseline nozzle and the nozzle with fluidic slot injection at several mass flow rates.

Figure 49 shows the pressure and axial velocity distributions at the centerline near the nozzle exit for both the baseline nozzle and the nozzle with the fluidic slot injection at various mass flow rates. It can be seen that shock cells of the nozzle with the fluidic injection move slightly upstream and the velocity magnitude at the centerline is lower, probably caused by the larger buildup of the high pressure. The pressure distributions for all cases except that of the highest injection flow rate follow a similar curve before the first compression wave arrives. This compression wave moves slightly upstream as the injection flow rate increases. The velocity magnitude for both injection flow rate at 0.0% and 1.06% is lower than that of the original CD nozzle, but the velocity magnitude of flow rate at 2.17% becomes higher. The injection flow rate at 8.80% completely alters the shock-cell structure inside nozzle. As mentioned above, the expansion wave emanating from the sharp throat has completely gone, and it suggests that the effective throat location has moved slightly behind the injection slot. In addition, the axial extent of the shock cells appears to be notably larger.

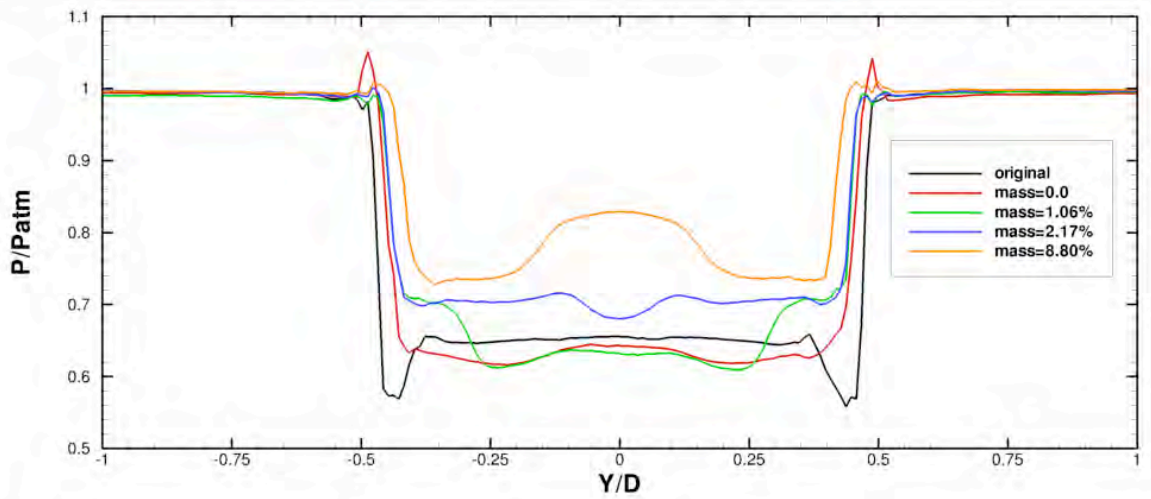

Figure 50. Static pressure distributions at nozzle exit for both the original nozzle and the nozzle with fluidic slot injection at several mass flow rates.

Figure 50 shows pressure profiles at the nozzle exit for the various cases. It can be seen that the pressure near the nozzle lip increases as the flow rate increases. This increase makes the pressure less over-expanded near the nozzle lip. The pressure around the center can be lower than that of the original value if the injection flow rate is low. However, as the injection flow rate increases, the static pressure reaches a higher value than that of the original C-D nozzle over the entire nozzle exit, such as observed for the case with the flow rate at 2.17%. This higher pressure makes the flow less over-expanded at the nozzle exit.

For the under-expanded jet case with NPR = 4.0, the observations are similar. The shock cells move slightly upstream and the buildup of the high pressure increases the size of the Mach disk, producing a larger wake region. As before, the pressure at the nozzle exit becomes more under-expanded for all the injection flow rates. Further analysis may show that this is an undesirable effect and we may need “suction” instead of “blowing” for noise reduction in the under-expanded jet cases.

Far-field acoustic testing was also performed for NPR of 2.5, 3.671 and 4.5 representing over-expanded, perfectly expanded and under-expanded jet cases respectively. Figure 51 shows the OASPL delta plot for a NPR of 2.5. The straight black line represents the baseline configuration. The blue line represents the area-ratio nozzle with the injection delivery system closed off. The remaining three lines correspond to increases in injection flow rate going from red to green. The mere presence of the injection slot has a beneficial effect in terms of noise production. The beneficial reduction of the slot is reduced with low injection amounts, but is further enhanced with the larger two amounts. The forward and side angles are most drastically affected and reductions of over 2dB are seen. In the aft angles there is reduced effectiveness and even noise production. Corresponding spectral plots are shown in Figure 52 for observation angles of 35°, 90°, and 140° measured from the upstream jet axis. In the forward angle there is low frequency and screech tone production, but ample noise reduction in the broadband shock associate noise and higher frequencies that improve with injection. The side angle shows similar trends, except there is a region of noise production in the higher frequencies. The noise

production seen in the aft angles in Figure 51 is explained by the large tonal peaks that are introduced within the spectrum at aft angles (Figure 52 c).

The NPR = 3.671 far field results (not shown) have similar trends but noise reduction is reduced to around 0.75dB. Figure 53 shows averaged shadowgraph images of the baseline nozzle and the injection nozzle with the injection turned on. The typical double diamond shock structure is seen in the baseline image. The flow field with injection = 0.49% has been modified in such a fashion that the double diamond structure has coalesced into a single shock diamond. Interestingly this injection rate corresponds to the optimum OASPL noise reduction condition, which suggests a shock cancellation phenomenon.

At a nozzle pressure ratio of 4.5 the noise benefits are all but eliminated. There is still some mid frequency reduction, but additional noise is created at all other frequencies. The beneficial shock cancelation that was experienced for NPR = 3.671 was unachievable with the air system in the ATF. Again for underexpanded operation it may be advantageous to employ suction instead of injection.

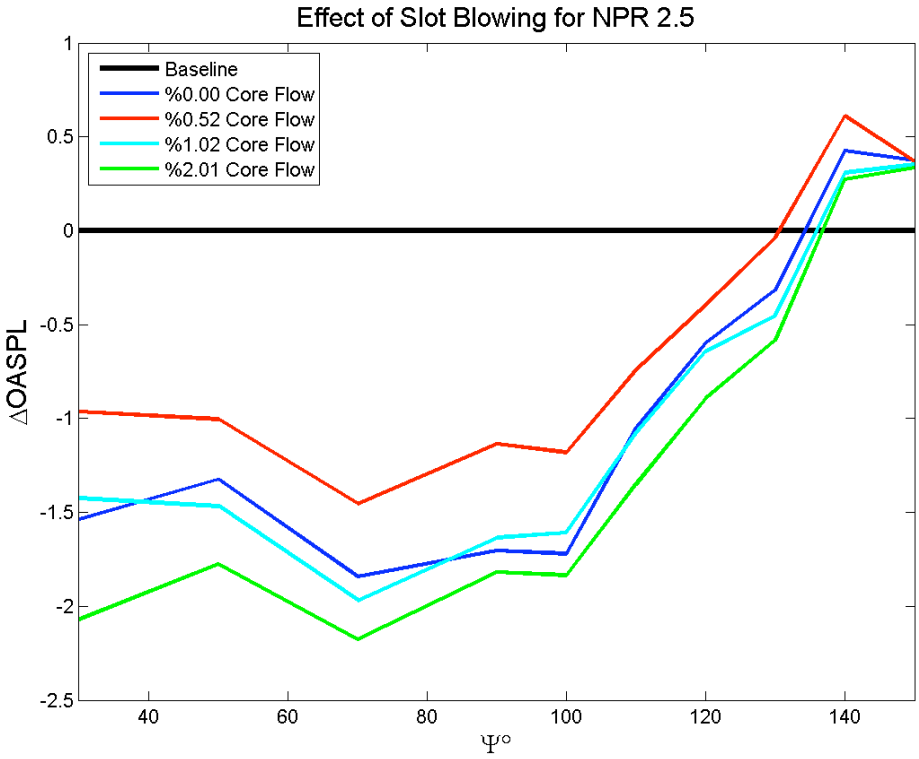

Figure 51. OASPL comparison between baseline (black), zero injection (blue), and several injection ratios expressed in percentages. The core jet NPR is 2.5.

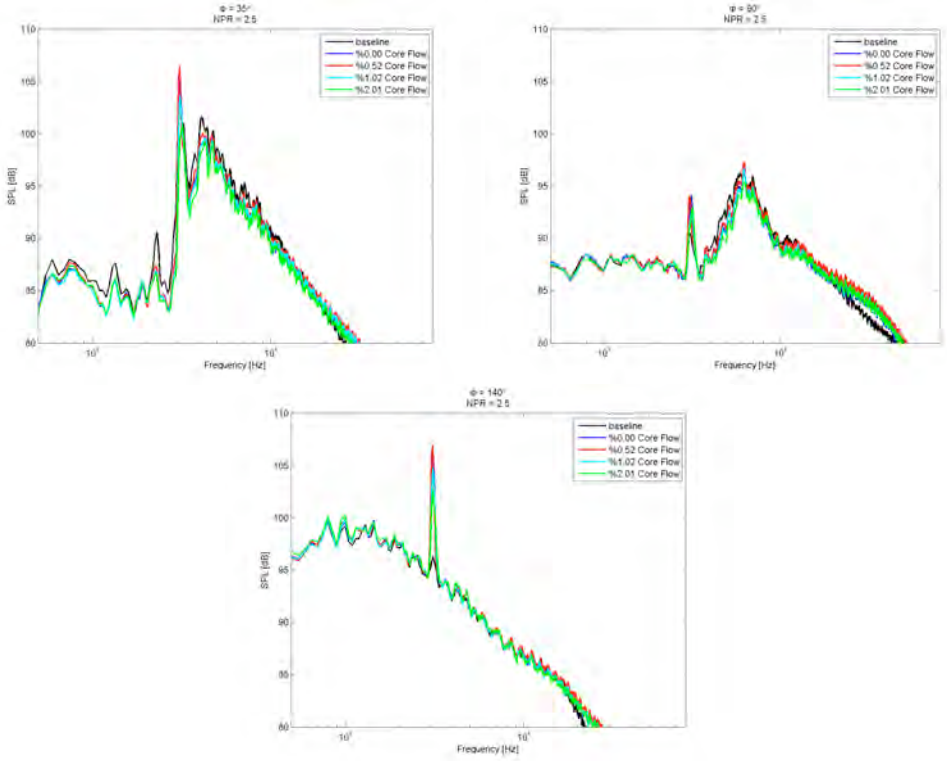

Figure 52. SPL spectra for NPR = 2.5 at observation angles of a.) 35°, b.) 90°, c.) 140° measured from the upstream jet axis.

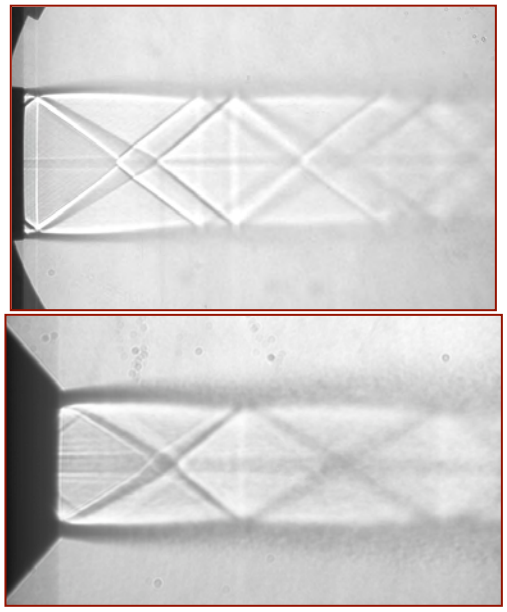

Figure 53. Averaged shadowgraph images of NPR = 3.671 a.) baseline b.) Injection = 0.49%

Summary of Observation on Fluidic Injection for Area-Ratio Control

In summary, fluidic injection through slots inside the nozzle is definitely effective in interacting with the shocks inside the nozzle divergent section. Analysis of the static pressure distributions at the nozzle exit indicate that as the injection flow rate increases, the static pressure also increases. For example, with a relatively modest injection mass flow rate of 2.17% (NPR = 2.5), the flow is less over-expanded at the nozzle exit than the baseline case. This is the effect we hypothesized originally and experimental results show a beneficial noise reduction. Furthermore the possibility of coalescing the double diamond shock structure and achieving shock cancelation through use of slot injection was found to be achievable and to correspond to the optimum noise reduction.

This study completed our investigation on the use of fluidic injection to reduce the noise from representative military-type jet aircraft engine nozzles. The next task was synthesizing the observations and providing recommendations. This is done in the next section of this document.

Task 4: Recommendations for Fluidics Based Noise Reduction

The fourth task was to synthesize results and develop recommendations. One of the deliverables under this task is a report on design recommendations for fluidics based noise reduction. This has been done separately and the information submitted is included here for completeness.

As planned, three fluidics-based noise reduction techniques were investigated in this project. To recapitulate, these were: 1) Replacing mechanical chevrons with fluidic injection; 2) Enhancing the effectiveness of mechanical chevrons by using fluidic injection along with the mechanical chevrons and 3) Using fluidic injection to effectively alter the throat to nozzle exit area-ratio. All three research activities were successfully completed.

Some of the key research accomplishments or observations on fluidics are:

1) The same-level of noise reduction as that achieved using mechanical chevrons can also be obtained using modest amounts (1-2 %) of fluidic injection of air. The further advantage of fluidic injection is that it can be turned on or off while mechanical chevrons are always present, once installed on the nozzle.
2) By carefully choosing and controlling the location and magnitude of fluidic injection, the effectiveness of mechanical chevrons can be further enhanced. However, if not carefully designed, the fluidic injection could counter some of the flow modification introduced by the chevrons and thus result in less noise reduction.
3) Fluidic injection can be effectively used to vary the area-ratio between the throat and exit areas and does modify the external shock-cell structure. However, results to date have shown only modest reduction in the near-field noise and in the far field noise (for certain operating conditions).
4) The injection geometries and chevrons employed in the study were chosen to ensure that significant effects would be present. The geometries were in no way optimized. Further systematic studies using the developed computational tool and complimentary

experiments are needed to optimize fluidic injection for noise reduction under various scenarios.

With the third fluidic injection technique (nozzle area-ratio variation), the pressure at the nozzle exit becomes more under-expanded for all the injection flow rates. In effect, further analysis shows that this is may be undesirable effect for jets that are already under-expanded and we may need “suction” instead of “blowing” for noise reduction in the under-expanded jet cases. This is a significant new finding. Far-field measurements show that for over-expanded jet cases the mere presence of the blowing slot even without mass flow reduces noise in the forward and sideline directions. Increasing mass flow though the slot then reduces noise further in these directions.

In summary, fluidic injection is a technically promising and an effective noise reduction technique. In general, fluidic injection in place of mechanical chevrons shows promise. For a constant injection mass flow, the effectiveness of fluidic injection decreases with increasing jet Mach number. Fluidic injection in combination with mechanical chevrons, in general, enhances the chevron effectiveness, especially at low values of jet Mach number. These are the Mach numbers where chevrons alone tend to be less effective. So fluidic injection does provide a complementary technique to mechanical chevrons for noise reduction. A key advantage of fluidic injection is that it can be easily turned on and off unlike mechanical chevrons, which are always present once installed on the nozzle and hence will modify the flow field under all operating conditions and will adversely affect engine performance. A disadvantage of fluidic injection is that more changes are required for retrofitting to existing engines than a chevron nozzle modification since an additional stream of air is required.

A recommendation to implement it either as a sole noise control technique or in conjunction with mechanical chevrons needs to also consider the total life-cycle costs involved with this as well as alternate techniques along with the benefits. The impact on performance of all options needs to be also considered. Fluidic injection is likely to alter the performance less than chevrons and may even increase it slightly under certain conditions because of the additional momentum due to fluidic injection.

Conclusions and Implications for Future Research

This is the final technical report on this project and covers the period from March 2007 to March 2010. All the work planned for this project has been successfully accomplished. The first sub-task was the verification and validation studies, which also had a go/no-go criterion. The verification studies included tests of the effects of grid resolution, mesh distribution, numerical parameters (e.g., flux limiters), domain size and various boundary conditions on the computed solutions. These studies showed that the solutions were computed accurately. For the validation studies, the computed solutions for both under-expanded and over-expanded jets were then compared with experimental data and shown to be in good to excellent agreement. The quantities compared included centerline pressure distributions, shock-cell size, size of the potential core, extent of jet mixing, Mach number distribution, shadowgraphs, noise spectra including key frequencies and characteristic differences in the flow field between under- and over-expansion. The ability of the simulations to characterize under- and over-expanded jets was demonstrated convincingly. This was the go/no-go decision point and after the 2008 IPR, the project was approved for continuation.

After the validation tests were completed, both the experiments and the numerical simulations were used to develop better physical understanding of the mechanisms of noise production and identify noise sources when a military aircraft engine is operating at ideal and non-ideal expansion conditions (over and under-expanded jet nozzle exhaust). This was the second task in the overall project and included three sub-tasks, which were all completed in a timely manner. Analysis of the sound production and radiation at several characteristic frequencies was carried out. An overlay of the narrow-band spectra at a characteristic noise source frequency showed a smooth transition from the computed solutions to the experimental data, indicating that both computations and experiments were capturing the same noise source. The smooth transition in the overlay is a significant accomplishment because experimentally it is not possible to interrogate the noise source non-intrusively and we must rely on the computations for this information. The perceived noise at a distance is a parameter that can be best measured experimentally and is prohibitively expensive to compute directly. This work further highlighted the complementary role of the experiments and simulations.

Cross-correlations of the pressure fluctuations outside the jet with the axial velocity fluctuations within the jet reveal that the screech tone is strongly related to the flow events occurring between the third shock cell and the end of the potential core. The shock-cell spacing itself increases as Nozzle Pressure Ratio (NPR) increases. This is consistent with the reduction in screech frequency noted with increasing NPR. Analysis of the sound pressure level distributions reveals that the low frequency noise dominates the mixing region downstream of the potential core. Overall, we find that noise generation from these jets can be categorized into three regions according to the noise generation mechanism: 1) near nozzle lip region and several diameters downstream, 2) further downstream in the region where the interaction between the shock cells and the large-scale coherent motions is large, and finally 3) the mixing region. The space-time correlation between the pressure above the nozzle exit and the shear stress 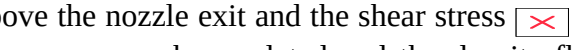 along the jet lip-line was studied. The first-order terms, mean shear related and the density-fluctuation related terms, are the main contributors to this correlation. Waves propagating upstream have a speed

slightly larger or very near the speed of sound, but the waves propagating downstream have a smaller speed, which increases as the radial distance increases and attains the sound speed at a certain radial distance. The time histories of static pressure along x lines (streamwise lines) reveal that the interaction between waves propagating in opposite directions produces waves with shorter streamwise wavelengths, and the locations of such waves move downstream as the radial distance increases. The work on the noise sources has been presented at scientific meetings and is being prepared for archival publication.

The next task was on investigating particular noise reduction techniques. First, we conducted experiments and simulations to assess the impact of mechanical chevrons on the flow field and near-field noise. Although the emphasis of our noise reduction strategy was based on fluidics, we needed to do these basic studies on chevrons to provide a baseline to evaluate the impact of fluidics-based techniques operating on chevrons. The results from our studies show that chevrons cause the shock cells to move closer to the nozzle and reduce the spacing between them. In addition, they induce more spread of the jet flow and decrease the strength of the shock cells. All these factors result in a reduction in the noise by more than 3 dB at the locations interrogated. The screech tone, which was so dominant in the baseline nozzle configuration, has been completely eliminated. Then three specific fluidic-based noise reduction techniques were investigated, as discussed in detail earlier in this report.

In general, fluidic injection in place of mechanical chevrons shows promise. For a constant injection mass flow, the effectiveness of fluidic injection decreases with increasing Jet Mach number. Fluidic injection in combination with mechanical chevrons, in general, enhances the chevron effectiveness, especially at low values of jet Mach number. These are the Mach numbers where chevrons alone tend to be less effective. So fluidic injection does provide a complementary technique to mechanical chevrons for noise reduction. A key advantage of fluidic injection is that it can be easily turned on and off unlike mechanical chevrons, which are always present once installed on the nozzle and hence will modify the flow field under all operating conditions. A disadvantage of fluidic injection is that more changes are required for retrofitting to existing engines than a chevron nozzle modification since an additional stream of air is required.

In conclusion, some of the key research accomplishments or observations from this project are:

1) Development of a validated computational capability for predicting the near-field noise generated by supersonic military aircraft jets under a variety of operating conditions, including non-ideally expanded jet nozzle conditions.
2) The observation that even when ideally expanded the flow field from typical military type jet exhaust nozzles are shock containing and produce shock associated noise because of the sharp throat present in these nozzles (due to other operational, manufacturing and maintenance requirements).
3) Mechanical chevrons are effective in reducing the noise level of supersonic jets under a variety of operating conditions.
4) Fluidically enhancing mechanical chevrons improves noise reduction while only employing a small amount of injection air (1-2%). For a substantially over-expanded jet, the case where the chevrons are least effective fluidic enhancement is greatest reducing by nearly 2 dB.

5) The same level of noise reduction as that achieved using mechanical chevrons can also be obtained using modest amounts (1-2 %) of fluidic injection of air. The further advantage of fluidic injection is that it can be turned on or off while mechanical chevrons are always present, once installed on the nozzle.
6) Fluidic injection can be effectively used to vary the area-ratio between the throat and exit areas and does modify the external shock-cell structure. However, results to date have shown only modest reduction in the near-field noise.
7) The injection geometries and chevrons employed in the study were chosen to ensure that significant effects would be present. The geometries were in no way optimized. Further systematic studies using the developed computational tool and complimentary experiments are needed to optimize mechanical chevrons and fluidic injection for noise reduction under various scenarios.

Literature Cited

1. Tam, C.K.W., and Tanna, H.K., Shock-Associated Noise of Supersonic Jets from Convergent-Divergent Nozzles," J. Sound Vib., Vol. 81, No. 3, pp. 337-358, 1982.
2. Norum, T.D., and Seiner, J.M., Broadband shock noise from supersonic jets, AIAA Journal, Vol. 20, No.1, pp. 68-73, 1982.
3. Seiner, J.M., Advances in High Speed Jet Aeroacoustics," AIAA Paper 84-2275, 1984.
4. Tam, C.K.W., Jet Noise Generated by large Scale Coherent Motion, Aeroacoustics of Flight vehicles: Theory and Practice, Vol. 1: Noise Sources, Edited by H.H. Hubbard, NASA RP-1258, pp. 311-390, 1991.
5. Tam, C.K.W., Supersonic Jet Noise, Annual Review of Fluid mechanics, Vol. 27, pp. 17-43, 1995.
6. Krothapalli, A., Soderman, P.T., Allen, C.S., Hayes, J.A., Jaeger, S.M, Flight effects on the far-field noise of a heated supersonic jet, AIAA Journal, Vol. 35, No.6, pp. 952-957, 1997.
7. Raman, G., Advances in Understanding Supersonic Jet Screech: Review and Perspective, Progress in Aerospace Sciences, Vol. 34, pp. 45-106, 1998.
8. Umeda, Y., and Ishii, R., On the sound sources of screech tones radiated from choked circular jets, J. Acoust. Soc. Am, 110 (4), 1845-1858, 2001.
9. Callender, B., Gutmark, E. and S. Martens, Far-Field Acoustic Investigation into Chevron Nozzle Mechanisms and Trends, AIAA Journal, Vol.43, no.1, pp.87-95, 2004.
10. Panda, J. Identification of noise sources in high speed jets via correlation Measurements - a review, AIAA-2005-2844, 2005.
11. DeBonis, J.R., and Scott, J.N., A large-eddy simulation of a turbulent compressible rounds jet, AIAA Paper 2001-2254, 2001.
11. Shur M.L., Spalart, P.R., Strelets, M., and Traven, A.K., Towards the prediction of noise from jet engines, Int. J. of Heat and Fluid Flow,Vol. 24, pp. 551-561, 2003.
12. Uzun, A., Lyrintzis, A.S., and Blaisdell, G.B., Coupling of integral acoustics methods with LES for jet noise prediction, Intnl. J. Aeroacoustics, Vol. 3, No. 4, pp. 297-346, 2004.
13. Kenzakowski, D.C., Kannepalli, C., and Brinckman, K.W., Computational Studies Supporting Concepts for Supersonic Jet Noise Reduction, AIAA Paper 2004-0518, 2004.
14. Bodony, D., and Lele, S., Review of the current status of jet noise predictions using Large Eddy Simulations, AIAA Paper 2006-486, 2006.

15. Shur, M.L., Spalart, P.R., Strelets, M.K., and Garbaruk, A.V., Further steps in LES-based noise prediction for complex jets, AIAA Paper 2006-485, 2006.
16. Berland, J., Bogey, C., and Bailly, C., Large eddy simulation of screech tone generation in a planar underexpanded jet, AIAA Paper 2006-2496, 2006.
17.Viswanathan, K., Shur, M.L., Spalart, P.R., and Strelets, M.K., Computation of the flow and noise of round and beveled nozzles, AIAA Paper 2006-2445, 2006.
18. Loh, C.Y., and Hultgren, L.S., Jet Screech Noise Computation, AIAA J, Vol. 44, No. 5, pp. 992-998, 2006.
19.DeBonis, J.R., Progress Toward Large-Eddy Simulations for Prediction of Realistic Nozzle Systems, J. Prop. Power, Vol. 23, No. 5, pp. 971-980, 2007.
20. Alkislar, M.B., Krothapalli, A., and Butler, G.W., The Effect of Streamwise Vortices on the Aeroacoustics of a Mach 0.9 Jet.", J. Fluid. Mech., v. 578, pp. 139-169.
21. Lo, S.C., Blaisdell, G.A., and Lyrintzis, A.S., Numerical Simulation of Supersonic Jet Flows and their Noise, AIAA Paper 2008-2970, 2008.
22. Eastwood, S., Tucker, P., and Xia, H., Comparison of LES to LDA and PIV Measurements of a Small Scale High Speed Coflowing Jet, AIAA Paper 2008-2981, 2008.
23. Kolbe, R., K. Kailasanath, K., Boris, J.P. and Young, T.R., Numerical Simulation of Flow Modification of a Supersonic Rectangular Jets, AIAA Journal, Vol. 34, No. 5, 1996.
24. Liu, J., Kailasanath, K., Ramamurti, R., Munday, D., Gutmark, E., and Lohner, R., Large-Eddy Simulation of a Supersonic Jet and Its Near-Field Acoustic Properties- Methodology & Validation, AIAA Paper 2009-0500, Presented at the 47th AIAA Aerospace Sciences Meeting, Orlando, FL, Jan 5-8, 2009, also published in the *AIAA Journal*, Vol. 47, pp. 1849-1864, 2009.
25. Munday, D., Gutmark. E., Liu, J., and Kailasanath, K. (2008) , Flow and Acoustic Radiation from Realistic Tactical Jet C-D Nozzles, AIAA-2008-2838.
26.Lighthill, M.J., On the sound generated aerodynamically: I, general theory, Proc. Royal Soc. London A, Vol. 211, pp. 564-587, 1952.
27. Ffowcs-Williams, J.E., and Hawkings, D.L., Sound Generated by Turbulence and Surfaces in Unsteady Motion, Phil. Trans. Royal Soc. London A, Vol. 264, No. 1151, pp. 321-342, 1969.
28. Lohner, R., FEM-FCT: Combining unstructured grids with high resolution, Communications in Applied Numerical Methods, Vol 4, pp. 717-729, 1998.
29. Boris, J.P. and Book, D.L., Flux-corrected Transport I:SHASTA a fluid transport algorithm that works, Journal of Computational Physics, Vol.11, 38, 1973.
30. Grinstein, F.F. and Fureby, C., On Monotonically Integrated Large Eddy Simulation of Turbulent Flows Based on FCT Algorithms, Chapter 3 in *Flux-Corrected Transport: Principles, Algorithms, and Applications* , Eds., D. Kuzmin, R. Lohner, and S. Turek, Springer, pp. 79-104, 2005.
31. Tam, C. K. W., Seiner, J. M., and Yu, J.C., Proposed Relationship between Broadband Shock Associated Noise and Screech Tones, *Journal of Sound and Vibration*, Vol. 110, No.2, pp. 309-321, 1986.
32. Alkislar, M., Choutapalli, C., Krothapalli, A., and Lourenco, L., "Structure of Supersonic Twin jets," AIAA Journal, Vol. 43, No. 11, pp. 2309-2318, 2005.

Appendix

List of Technical Publications and Presentations:

1. Journal Articles:

"Large-Eddy Simulation of a Supersonic Jet and Its Near-Field Acoustic Properties," Liu, J., Ramamurti, R., Kailasanath, K., Munday, D., Gutmark, E, and Lohner, R., *AIAA Journal*, Vol. 47, 2009, pp. 1849-1864.
(**received a 2009 Alan Berman Research Publication Award by NRL)**

"Supersonic Jet Noise Reduction Technologies for Gas Turbine Engines, " Munday, D., Heeb, N., Gutmark. E., Liu, J., and Kailasanath, K., *Journal of Engineering for Gas Turbines and Power*, Vol. 133, No. 7, to appear, July 2011.

2. Conference proceedings:

Flow and Acoustic Radiation from Realistic Tactical Jet C-D Nozzles," Munday, D., Gutmark, E., Liu, J., Kailasanath, K., 14th AIAA/CEAS Aeroacoustics Conference, 5 May 2008, Vancouver, British Columbia, Canada, AIAA-2008-2838.

"Large-Eddy Simulation of a Supersonic Jet and Its Near-Field Acoustic Properties :Methodology and Validation," Liu, J., Kailasanath, K., Ramamurti, R., Munday, D., Gutmark, E., Lohner, R., 47th AIAA Aerospace Sciences Meeting, 5 Jan 2009, Orlando FL, AIAA-2009-0500.

"Investigation of Near-Field Acoustic Properties of Imperfectly Expanded Jet Flows Using LES," Liu, J., Kailasanath, K., Munday, D., Gutmark, E., 47th AIAA Aerospace Sciences Meeting, 5 Jan 2009, Orlando FL, AIAA-2009-0015.

"Acoustic Effect of Chevrons on Jets Exiting Conical C-D Nozzles," Munday, D., Heeb, N., Gutmark, E., Liu, J., Kailasanath, K., 15th AIAA/CEAS Aeroacoustics Conference, 11 May 2009, Miami, FL, AIAA-2009-3128.

"Large-Eddy Simulations of Imperfectly Expanded Jets from a Chevron Nozzle," Liu, J., Kailasanath, K., Ramamurti, R., Munday, D., Gutmark, E., 15th AIAA/CEAS Aeroacoustics Conference, 11 May 2009, Miami, FL, AIAA-2009-3192.

"Flow Structure of Supersonic Jets from Conical C-D Nozzles," Munday, D., Gutmark, E., Liu, J., Kailasanath, K., 39th AIAA Fluid Dynamics Conference, 24 June 2009, San Antonio, Texas, AIAA-2009-4005

"Impact of Mechanical Chevrons on Supersonic Jet Flow and Noise," Kailasanath, K., Liu, J., Gutmark, E., Munday, D., Martens, S., ASME Turbo Expo 2009, 8-12 June 2009,

Orlando, FL, ASME-GT2009-59307. (**Work reported in this paper was selected as a Top 20 Research Accomplishment of 2009).**

"An Application of Commercial Noise Reduction Techniques to Military Aircraft Nozzles," Heeb, N., Munday, D., Gutmark, E., Liu, J., Kailasanath, K., 48th AIAA Aerospace Sciences Meeting, 5 Jan 2010, Orlando FL, AIAA-2010-0656.

"Fluidic Injection for Noise Reduction of a Supersonic Jet from a practical C-D nozzle," Munday, D., Heeb, N., Gutmark, E., Liu, J., Kailasanath, K., 16th AIAA/CEAS Aeroacoustics Conference, Stockholm, Sweden, AIAA 2010-4024, June 2010.

"Large-Eddy Simulations of a Supersonic Jet with Fluidic Injection for Noise Reduction," Liu, J., Kailasanath, K., Ramamurti, R., Munday, D., Gutmark, 16th AIAA/CEAS Aeroacoustics Conference, Stockholm, Sweden, AIAA 2010-4028, June 2010.

"Supersonic Jet Noise Reduction using Fluidics, Mechanical Chevrons and Fluidically Enhanced Chevrons," Munday, D., Heeb, N., Gutmark, E., Liu, J., Kailasanath, K., ASME Turbo Expo 2010, Glasgow, Scotland, 14-18 June 2010.

"Supersonic Jet Noise Reduction by Chevrons Enhanced with Fluidic Injection," Heeb, N., Munday, D., Gutmark, E. Liu, J., and Kailasanath, K., 40th AIAA Fluid Dynamics Conference, Chicago, Illinois, 28 June – 1 July 2010.

3. Presentations:

"Acoustic Radiation from Imperfectly Expanded Supersonic Jets; Experimental Investigation," Munday, D., Gutmark., Liu, J., Kailasanath, K., presented at the Sixtieth Annual Meeting of the American Physical Society, Division of Fluid Mechanics, 19 November 2007, Salt Lake City, Utah.

"LES of the Flow Dynamics and Near-Field Acoustics of Non-Ideally Expanded Jets," Kailasanath, K., J. Liu, and R. Ramammurti, presented at the International Conference on Jets, and Shear flows , Berlin, Germany, September 2008.

" Investigation of the Near-Field Acoustic Properties of Imperfectly Expanded Supersonic Jets By PIV," Munday, D., Gutmark, E., Liu, J., and Kailasanath, K. presented at the 61st Annual Meeting of the Division of Fluid Dynamics, Bulletin of the American Physical Society, Vol. 53, November 2008.

"Investigation of the Near-Field Acoustic Properties of Imperfectly Expanded Supersonic Jets By LES," Liu, J., Ramamurti, R., Kailasanath, K., Munday, D., and Gutmark, E,

presented at the 61st Annual Meeting of the Division of Fluid Dynamics, Bulletin of the American Physical Society, Vol. 53, November 2008.

"MILES of the Flow Dynamics and Near-Field Acoustics of Supersonic Jets," Kailasanath, K., J. Liu, and R. Ramammurti, presented at the International Conference on Recent Advances in Combustion and Noise, Kauai, December 2008.

"Investigation of Near-Field Acoustic Properties of Imperfectly Expanded Jet Flows Using LES," Liu, J., Kailasanath, K., Munday, D., Gutmark, E., presented at the 47th AIAA Aerospace Sciences Meeting, AIAA-2009-0015, Orlando, FL., January 2009.

"Large-Eddy Simulation of a Supersonic Jet and Its Near-Field Acoustic Properties :Methodology and Validation," Liu, J., Kailasanath, K., Ramamurti, R., Munday, D., Gutmark, E., Lohner, R., presented at the 47th AIAA Aerospace Sciences Meeting, AIAA-2009-0500, Orlando, FL., January 2009.

"Acoustic Effect of Chevrons on Jets Exiting Conical C-D Nozzles," Munday, D., Heeb, N., Gutmark, E., Liu, J., Kailasanath, K., presented at the 15th AIAA/CEAS Aeroacoustics Conference, AIAA-2009-3128, Miami, FL., May 2009.

"Large-Eddy Simulations of Imperfectly Expanded Jets from a Chevron Nozzle," Liu, J., Kailasanath, K., Ramamurti, R., Munday, D., Gutmark, E., presented at the 15th AIAA/CEAS Aeroacoustics Conference, AIAA-2009-3192, Miami, FL., May 2009.

"Flow Structure of Supersonic Jets from Conical C-D Nozzles," Munday, D., Gutmark, E., Liu, J., Kailasanath, K., 39th AIAA Fluid Dynamics Conference, AIAA-2009-4005.
"Impact of Mechanical Chevrons on Supersonic Jet Flow and Noise," Kailasanath, K., Liu, J., Gutmark, E., Munday, D., Martens, S., presented at the ASME Turbo Expo 2009, ASME-GT2009-59307, Orlando, FL.

"Investigation of the Acoustic Properties of Supersonic Jets with Fluidic Injection on Chevrons: Experimental Results," Munday, D., Heeb, N., Gutmark, E., Liu, J., Kailasanath, K., presented at the Sixty-Second Annual Meeting of the American Physical Society, Division of Fluid Mechanics, 24 November 2009, Minneapolis, Minnesota.

"An Application of Commercial Noise Reduction Techniques to Military Aircraft Nozzles," Heeb, N., Munday, D., Gutmark, E., Liu, J., Kailasanath, K., presented at the 48th AIAA Aerospace Sciences Meeting, 5 Jan 2010, AIAA-2010-0656, Orlando, FL.

"Fluidic Injection for Noise Reduction of a Supersonic Jet from a practical C-D nozzle," Munday, D., Heeb, N., Gutmark, E., Liu, J., Kailasanath, K., presented at the 16th AIAA/CEAS Aeroacoustics Conference, Stockholm, Sweden 7-9 June 2010.

"Large-Eddy Simulations of a Supersonic Jet with Fluidic Injection for Noise Reduction," Liu, J., Kailasanath, K., Ramamurti, R., Munday, D., Gutmark, presented at the 16th AIAA/CEAS Aeroacoustics Conference, Stockholm, Sweden 7-9 June 2010.

"Supersonic Jet Noise Reduction using Fluidics, Mechanical Chevrons and Fluidically Enhanced Chevrons," Munday, D., Heeb, N., Gutmark, E., Liu, J., Kailasanath, K., presented at ASME Turbo Expo 2010, Glasgow, Scotland, 14-18 June 2010.

"Supersonic Jet Noise Reduction by Chevrons Enhanced with Fluidic Injection," Heeb, N., Munday, D., Gutmark, E. Liu, J., and Kailasanath, K., presented at 40th AIAA Fluid Dynamics Conference, Chicago, Illinois, 28 June – 1 July 2010.

4. Conference Posters:

"Double Diamonds and the Sound of Freedom: Jet Flows and Acoustic Emissions from Practical Military Engine Nozzles," Munday, D., Heeb, N., Gutmark, E., Kailasanath, K., Liu, J., University of Cincinnati Graduate School, 2010 Poster Forum, Cincinnati, Ohio, 5 March 2010.
(awarded Best in Natural Science and Engineering)